Cell Reports

Article

Golgi satellites are essential for polysialylation of NCAM and expression of LTP at distal synapses

Graphical abstract

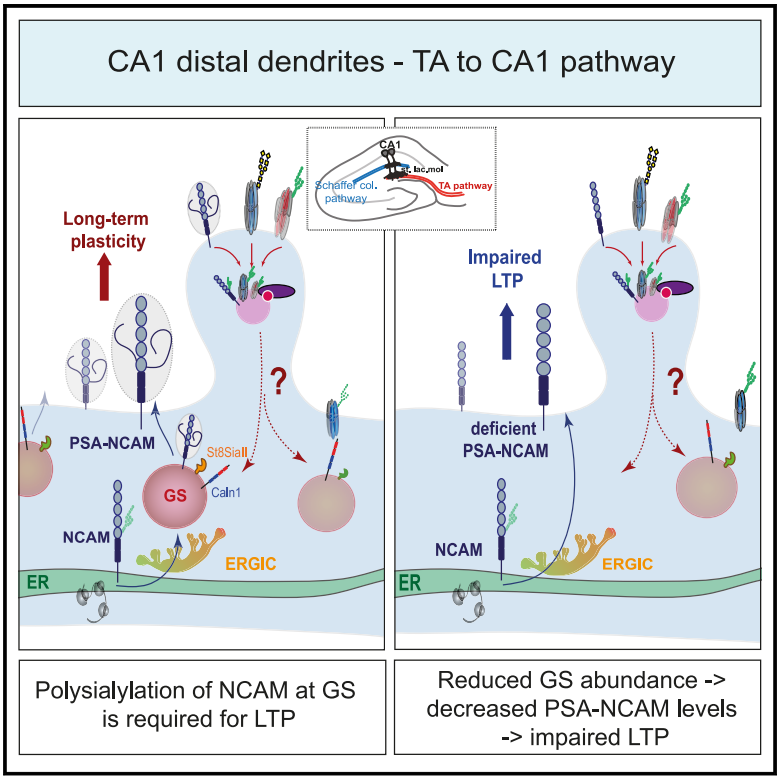

Highlights

- Golgi satellites (GSs) have features of TGN membranes and are widely distributed
- *De novo* glycosylation, including sialylation, occurs at Golgi satellites
- GSs are essential for NCAM polysialylation at distal dendrites of pyramidal neurons
- LTP expression is impaired in distal dendrites with fewer GSs and reduced PSA-NCAM

Authors

Maria Andres-Alonso, Maximilian Borgmeyer, Hadi Mirzapourdelavar, ..., Anja M. Oelschlegel, Alexander Dityatev, Michael R. Kreutz

Correspondence

maria.andres-alonso@zmnh.uni-hamburg.de (M.A.-A.), michael.kreutz@zmnh.uni-hamburg.de (M.R.K.)

In brief

Maturation of locally secreted proteins is challenged by the polarized morphology of neurons and the somatic localization of the Golgi apparatus. Andres-Alonso et al. show that dendritic Golgi satellites are capable of complex glycosylation and that polysialylation of NCAM at these organelles is essential for long-term plasticity at distal synapses.

Andres-Alonso et al., 2023, Cell Reports *42*, 112692
July 25, 2023
https://doi.org/10.1016/j.celrep.2023.112692

CellPress

Cell Reports

CellPress
OPEN ACCESS

Article

Golgi satellites are essential for polysialylation of NCAM and expression of LTP at distal synapses

Maria Andres-Alonso,[1,2,8,*] Maximilian Borgmeyer,[1,2,8] Hadi Mirzapourdelavar,[5] Jakob Lormann,[1,2] Kim Klein,[1] Michaela Schweizer,[3] Sabine Hoffmeister-Ullerich,[4] Anja M. Oelschlegel,[2] Alexander Dityatev,[5,6,7] and Michael R. Kreutz[1,2,5,6,9,*]

[1]Leibniz Group "Dendritic Organelles and Synaptic Function," Center for Molecular Neurobiology (ZMNH), University Medical Center Hamburg-Eppendorf, 20251 Hamburg, Germany
[2]RG Neuroplasticity, Leibniz Institute for Neurobiology, 39118 Magdeburg, Germany
[3]Core Facility Morphology und Electron Microscopy, Center for Molecular Neurobiology (ZMNH), University Medical Center Hamburg-Eppendorf, 20251 Hamburg, Germany
[4]Core Facility Bioanalytik, Center for Molecular Neurobiology (ZMNH), University Medical Center Hamburg-Eppendorf, 20251 Hamburg, Germany
[5]German Center for Neurodegenerative Diseases (DZNE), 39120 Magdeburg, Germany
[6]Center for Behavioral Brain Sciences, Otto von Guericke University, 39120 Magdeburg, Germany
[7]Medical Faculty, Otto von Guericke University, 39120 Magdeburg, Germany
[8]These authors contributed equally
[9]Lead contact
*Correspondence: maria.andres-alonso@zmnh.uni-hamburg.de (M.A.-A.), michael.kreutz@zmnh.uni-hamburg.de (M.R.K.)
https://doi.org/10.1016/j.celrep.2023.112692

SUMMARY

The complex cytoarchitecture of neurons poses significant challenges for the maturation of synaptic membrane proteins. It is currently unclear whether locally secreted synaptic proteins bypass the Golgi or whether they traffic through Golgi satellites (GSs). Here, we create a transgenic GS reporter mouse line and show that GSs are widely distributed along dendrites and are capable of mature glycosylation, in particular sialylation. We find that polysialylation of locally secreted NCAM takes place at GSs. Accordingly, in mice lacking a component of *trans*-Golgi network-to-plasma membrane trafficking, we find fewer GSs and significantly reduced PSA-NCAM levels in distal dendrites of CA1 neurons that receive input from the temporoammonic pathway. Induction of long-term potentiation at those, but not more proximal, synapses is severely impaired. We conclude that GSs serve the need for local mature glycosylation of synaptic membrane proteins in distal dendrites and thereby contribute to rapid changes in synaptic strength.

INTRODUCTION

The morphological complexity of principal neurons poses a fundamental challenge for trafficking and proteostasis of synaptic membrane proteins.[1–3] In recent years, a satellite microsecretory system was identified in neuronal processes that even allows for local synthesis and processing of transmembrane proteins. The endoplasmic reticulum (ER) in pyramidal neurons of the hippocampus is continuous between dendrites, a subset of spines, and the outer nuclear membrane, and dendrites contain the ER-Golgi intermediate compartment (ERGIC), retromer, dendritic mRNA, polyribosomes, and various other organelles and components for secretory trafficking.[1,2,4–6] It is thus likely that these microsecretory systems have acquired features to serve the specific requirements of synaptic communication, and it is therefore unfortunate that we still know very little about them.

One central and yet unanswered question is whether post-ER carriers require a Golgi-related compartment for glycosylation. Published evidence of highly abundant immature glycosylated profiles at the neuronal plasma membrane suggests that many proteins might bypass the Golgi.[7,8] Along these lines, in dendrites of mammalian neurons, only very few discontinuous structures resembling Golgi cisternae are present, and these are known as Golgi outposts.[5,9] In hippocampal pyramidal neurons, they either represent extended Golgi in the apical proximal dendrite of only a subset of cells or at branch points of the primary apical dendrite during dendritogenesis.[4,9] The low abundance of Golgi outposts in mammalian neurons[4,9] suggests that locally synthesized proteins in most distal dendrites might not undergo all processing steps of the canonical secretory pathway, and in consequence, those proteins could be functionally different from somatically synthesized proteins. Thus, faster

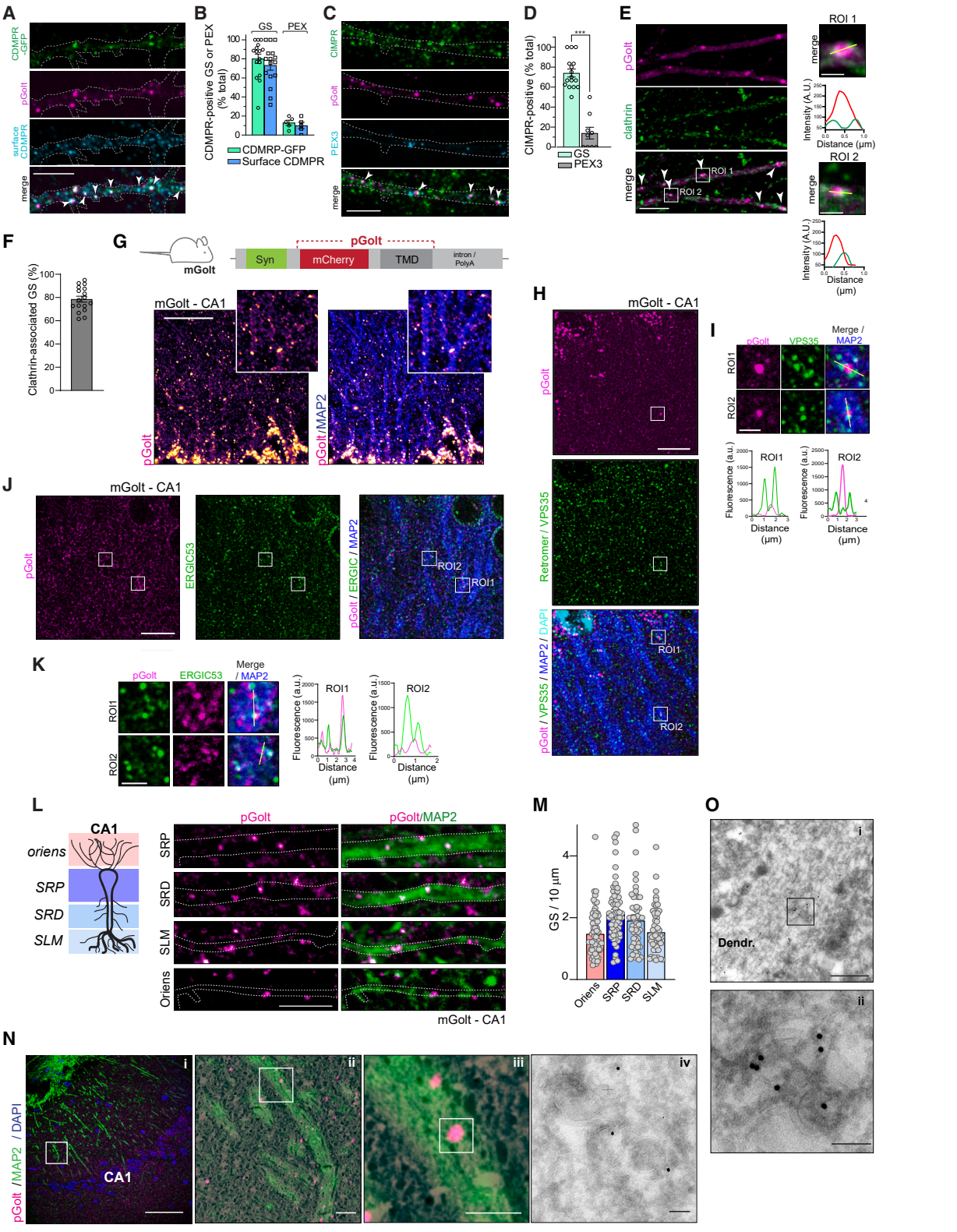

(legend on next page)

and spatially restricted delivery might come at the expense of functional maturity and protein stability.[3,5,7–9]

However, it is also becoming increasingly clear that different secretory routes exist that involve trafficking through different organelle networks.[7,8,10–13] Contrary to the view outlined above, we have provided evidence for the presence of a Golgi-related satellite microcompartment that is located at the interface of the ERGIC and retromer and that exhibits a widespread distribution in basal and apical dendrites.[13] Golgi satellites (GSs) lack Golgi matrix components and a stack structure typical of somatic Golgi, but they contain glycosylation machinery and synaptic transmembrane proteins that pass through and recycle back to GSs.[13] Evidence is currently sparse, however, on whether GSs indeed serve as local glycosylation platforms where synaptic membrane proteins could undergo maturation at distal dendrites. Moreover, to what extent glycosylation of synaptic membrane proteins at GSs contributes to molecular changes at synapses undergoing plasticity is currently unclear. Given this paucity of data, the relevance and even the mere existence of Golgi-related microcompartments in dendrites of mammalian neurons have been questioned.[5,7]

RESULTS

Dendritic GSs exhibit Golgi characteristics

We therefore first sought to resolve existing ambiguities about the existence of GSs by assessing their membrane characteristics. Here, we took advantage of two cargoes that reside in the *trans*-Golgi network (TGN), from where they continuously cycle to endosomes and the plasma membrane to eventually return to the TGN. The cation-dependent and cation-independent mannose-6 phosphate receptors (CD- and CIMPRs) mediate the segregation of newly synthesized lysosomal hydrolases from the secretory pathway and their delivery to endosomes, from which they return to the TGN for subsequent rounds of recycling.[14] Most important, the lower pH found in endosomal compartments triggers the dissociation of both receptors from their ligands, and the absence of MPRs clearly distinguishes lysosomal from Golgi-related membranes.[15] Expression of CDMPR-GFP (Figures 1A and 1B) as well as immunolabeling of endogenous CIMPRs (Figures 1C and 1D) in primary neurons resulted in a punctate distribution. We next assessed the localization of CDMPR-GFP and CIMPRs in GSs detected with the Golgi tracker pGolt,[13] which is tagged with the fluorescent protein mCherry and efficiently labels GSs.[13] We found that CD- and CIMPRs highly localize at GSs and that ~80% of GSs contained either CD- (Figures 1A and 1B) or CIMPRs (Figures 1C and 1D). Importantly, CIMPRs did not localize at peroxisomesidentified by expression of PEX3-Emerald and used as negative control for pGolt localization (Figures 1C and 1D). Finally, surface labeling of CDMPR-GFP located at the plasma membrane using an antibody against GFP in living neurons revealed that >75% of GSs contain internalized CDMPR-GFP (Figures 1A and 1B). This indicates that GSs also receive retrograde cargo from the plasma membrane that is known to fuse with TGN membranes.[15]

A distinctive feature of the *trans*-most TGN is the presence of clathrin, which can coat long areas of the cisternal part in the somatic TGN and also associates with TGN tubules, where it participates in the generation of post-Golgi carriers.[16] Immunocytochemical labeling of endogenous clathrin revealed that GSs labeled by pGolt are almost invariably associated with clathrin (Figures 1E and 1F). Taken together, the presence of clathrin as well as the directed trafficking of MPRs provide compelling evidence that GSs share characteristics of TGN membranes.

Figure 1. Dendritic GSs exhibit characteristics of TGN membrane and show a widespread distribution in the brain

(A) Representative images showing GSs labeled by pGolt-mCherry positive for CDMPR-GPF as well as surface-labeled CDMPRs from primary hippocampal neurons. Scale bar is 5 μm.

(B) Percentage of GSs and peroxisomes (PEXs) positive for CDMPR-GFP and surface CDMPRs from (A) (GS/CDMPR-GPF: n = 16; GS/surface CDMPR, n = 16; PEX14/CDMPR-GFP n = 5; PEX14/surface CDMPR: n = 5; two independent cultures).

(C) Representative images showing GS labeled by pGolt-mCherry or PEXs (PEX3) and endogenous CIMPRs. PEXs (PEX3) were used as negative control. Scale bar is 5 μm.

(D) Percentage of GSs or PEXs positive for CIMPR from (C) (GS/CIMPR n = 16 from four independent cultures; PEX3/CIMPR n = 9 from 3 independent cultures; unpaired t test, ***$p < 0.0001$).

(E) Representative images of primary hippocampal neurons expressing pGolt-mCherry and stained against clathrin. Regions of interest (ROIs) are shown amplified on the right together with the corresponding line profile. Scale bars are 5 and 1 μm (insets).

(F) Percentage of GSs associated with clathrin (n = 17 from 2 independent cultures).

(G) Scheme depicting the construct used to create the mGolt mouse line by random integration. Below, an overview of the CA1 region of the hippocampus from an mGolt mouse. Scale bar is 200 μm. See also Figures S1A–S1I.

(H) Representative images of cryosections from mGolt mice stained against the core component of retromer VPS-35, MAP2, and DAPI. An antibody against RFP/mCherry was used to boost the fluorescence signal from pGolt-mCherry. Scale bar is 10 μm.

(I) ROIs depicted in (H) and their corresponding fluorescence intensity line profiles below. Scale bar is 2 μm.

(J) Representative images of cryosections from mGolt mice stained against ERGIC53 and MAP2. Scale bar is 10 μm.

(K) Images from the ROIs depicted in (J) and their corresponding fluorescence intensity line profiles below. Scale bar is 2 μm.

(L) Left, cartoon depicting the different strata found in CA1. Right, representative images of GSs in dendrites labeled by MAP2. SRP, stratum radiatum proximal; SRD, stratum radiatum distal; SLM, stratum lacunosum moleculare. Scale bar is 5 μm.

(M) Quantification of dendritic GS/10 μm in each strata from the experiment in (H) ($n \geq 37$ dendrites from 2 animals per stratum). See also Figures S1E–S1G.

(N) Images from a CLEM experiment. (i) confocal overview of the CA1 region in mGolt brain sections stained with MAP2 and DAPI; (ii) overlay of the fluorescence image on the electron micrograph from the boxed area in (i) (scale bar is 2 μm); (iii) zoomed-in image from the box in (ii); and (iv) electron micrograph showing the ultrastructure and immunogold labeling of the GS in (iii) (scale bar is 100 nm).

(O) Electron micrographs of a dendrite in the CA1 region of a mGolt mouse (i). (ii) shows an amplified imaged from the region in (i). Scale bars are 500 and 200 nm, respectively. See also Figures S1K and S1L.

GSs appear as vesicular clusters and are widely distributed in the mouse brain

We next aimed to characterize the structure and function of GSs *in vivo*. To this end, we generated a transgenic mouse line by random integration of a construct encoding pGolt, which was tagged with the fluorescent protein mCherry.[13] In this mouse line that we named mGolt, the selective neuronal expression of the Golgi reporter is controlled by a synapsin promoter (Figures 1G, S1A, and S1B). Immunoblot analysis of mGolt mouse brains revealed prominent expression in the cortex and hippocampus (Figure S1C). Transgene expression had no effect on the ultrastructure of the secretory system, in particular not on the TGN, in the CA1 region of the hippocampus (Figure S1D). Analysis of mGolt fluorescence in hippocampal sections unveiled the presence of single, punctate structures that homogeneously decorated dendrites in pyramidal neurons of the CA1 region (Figure 1G) and that were found in very close association to VPS35 (Figures 1H and 1I) and ERGIC53 (Figures 1J and 1K), which are markers of the secretory compartments retromer and ERGIC, respectively, as described in primary neurons.[13] The subsequent quantification of GS distribution throughout the different CA1 strata in mGolt mice revealed similar results like in primary neurons upon expression of pGolt (Figures 1L and 1M).[13] Accordingly, GSs were uniformly distributed along dendrites with a density of ~2 GSs per 10 μm, and their localization was not restricted to or more prominent in proximal dendrites (Figures 1L and 1M). Thus, GSs were found in distal dendrites of the stratum lacunosum moleculare (SLM) with the same abundance as in more proximal dendritic segments (Figures 1L and 1M). pGolt fluorescence in mGolt animals is not restricted to pyramidal neurons, and expression of the Golgi tracker was detected in other brain areas such as the hippocampal dentate gyrus (Figures S1E and S1F). Analysis of GS distribution in dendrites of granule cells revealed that, similarly to what is found in CA1 pyramidal neurons, GSs are present at a frequency of ~2 GS/10 μm in granule cells (Figures S1F and S1G), suggesting that the number of GSs in a given dendrite does not correlate with dendritic arborization patterns but with dendritic length. As expected, pGolt fluorescence in pyramidal neurons was also present in the perinuclear region in close proximity to the *cis*-Golgi marker GM130 (Figure S1H), and the expression overlapped with the TGN marker Syntaxin 6 in the soma (Figure S1I).

In previous work, super-resolution scanning transmission electron microscopy (STED) microscopy revealed that GSs in dendrites of primary neurons are of diverse sizes and shapes that often show an irregular and extended morphology.[13] We next analyzed the ultrastructural characteristics of GSs in the brain by performing correlative light-electron microscopy (CLEM) in the stratum radiatum of CA1 hippocampal sections from the mGolt line (Figure 1Ni–1Niii), which we incubated with an antibody against RFP/mCherry coupled to colloidal gold to confirm the fluorescence data by immuno-EM (Figure 1Niv). pGolt-positive spots in distal MAP2-labeled dendrites were first detected with confocal microscopy (Figures 1Ni–1Niii), and the ultrastructure of the corresponding region was further assessed by EM (Figure 1Niv). Fluorescence structures were analyzed from >3 independent experiments, and only fluorescent spots with a well-defined underlying ultrastructure that correlated with the presence of colloidal gold particle clusters were considered. Overall, ~10% of all pGolt-mCherry-positive spots analyzed were considered positive, a fact that we believe is due to the technical challenges of the methodology and the selection criteria used. In line with previous work, ultrastructural analysis of these fluorescent- and gold-positive GSs revealed the absence of Golgi cisternae characteristic of Golgi stacks (Figures 1Niv–1O and S1J).[13] Instead, the fluorescent signal associated with GSs originally identified by confocal microscopy correlated with the presence of irregular clusters of pleomorphic vesicle-like structures that lack any sign of electron-dense material (Figures 1N, 1O, and S1J). These heterogeneous structures show a non-spherical shape and vary in size, altogether having a dimension of several hundred nanometers, and may result from the cross-section of clathrin-positive branched tubules characteristic of TGN membranes (Figures 1E and 1F).[16] Expectedly, we found prominent immunogold labeling at the somatic TGN as a result of the efficient targeting of pGolt to TGN membranes (Figure S1K).[13] Taken together, these results indicate that TGN-related dendritic membrane structures are labeled in brains of mGolt mice. Moreover, GSs are widely distributed along dendrites and appear as heterogeneous pleiomorphic clusters.

GSs bear *de novo* N- and O-glycosylated proteins

Golgi-resident enzymes include transmembrane proteins that catalyze the formation of long sugar chains attached to their substrate. This typically requires their organized localization along the Golgi stacks, which reflects the sequential order of the sugar-adding reactions they execute, although this position is not static, as it is influenced by the flux of traffic.[17,18] In light of this, we next asked whether glycosylation can occur at GSs and, if so, which type of glycosylation is carried out at these microcompartments. To investigate this question, we first employed biotin-coupled lectins in rat primary cultures expressing pGolt-mCherry. Lectins are specific sugar-binding proteins involved in recognition of different types of glycans (Figures 2A and 2B).[19] *Concanavalin A* (ConA) was used to detect core-glycosylated—often called immature-glycosylated—proteins. These proteins carry a mannose-rich residue added in the ER lumen that typically undergoes further processing in subsequent steps at the Golgi.[8,19] Wheat germ agglutinin (WGA) labels complex N-glycosylated proteins and sialic acid residues,[8,20] whereas *Helix pomatia* (*HPL*) detects proteins carrying O-linked glycans.[21] Quantification of the percentage of positive GSs revealed that the great majority of GSs (~88%) contained core-glycosylated proteins (Figures 2A and 2B), in agreement with the presence of immature-glycosylated secretory cargoes that enter GSs for further processing. Similarly, the vast majority (~79%) of GSs found in dendrites of the stratum radiatum in the CA1 region of mGolt mice are also enriched in glycosylated proteins labeled by ConA (Figures 2C and 2D). In addition to core-glycosylated proteins, ~81% of GSs in primary neurons were found to be enriched in complex N-glycosylated proteins including those containing sialic acid, and O-glycosylated proteins labeled by HPL were also found to be abundant in ~60% of the analyzed GSs (Figures 2A and 2B). Moreover, treatment with tunicamycin, an

CellPress
OPEN ACCESS

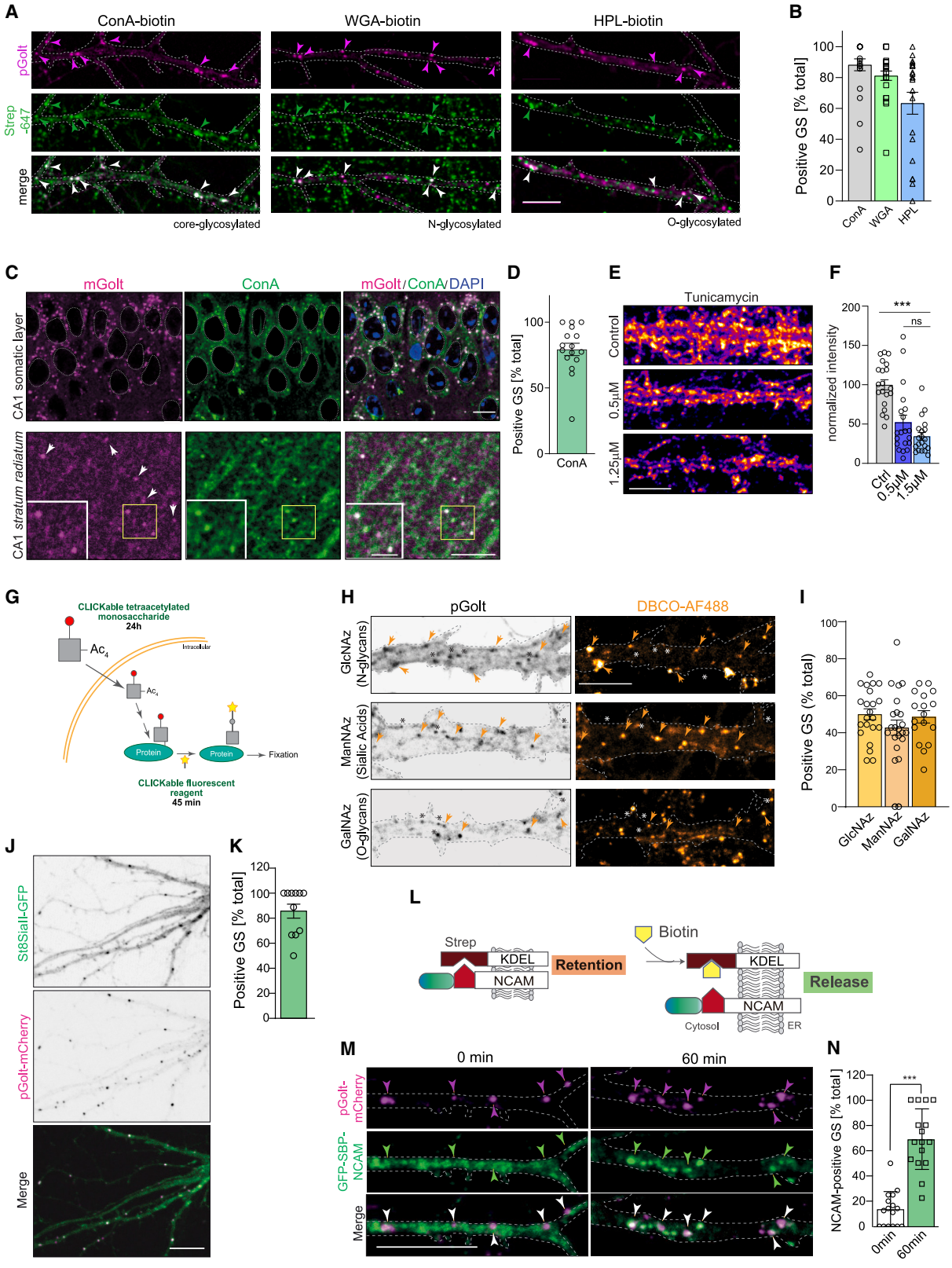

(legend on next page)

antibiotic that prevents the transfer of the N-glycan precursor in the early glycosylation steps at the ER, diminished ConA fluorescence intensity in dendrites (Figures 2E and 2F), indicating specificity of labeling. Collectively, these results support a function of GSs in complex glycosylation of proteins.

In order to obtain direct evidence for the involvement of GSs in glycosylation of locally secreted proteins in dendrites, we performed metabolic labeling using azido-modified monosaccharides that are incorporated into the target glycan and are visualized in a second step by a covalent reaction with an imaging probe (Figure 2G).[23–25] Neurons expressing pGolt were incubated for 24 h with different azide sugars. We employed tetraacetylated N-azidoacetyl-glucosamine (Ac_4GlcNAz) and N-azidoacetyl-galactosamine (Ac_4GalNAz) to label most prominently N- and O-linked glycans, respectively. Additionally, N-azidoacetyl-mannosamine (Ac_4ManNAz) was employed to specifically label sialic acids, which are a family of nine-carbon monosaccharides that decorate N- and O-linked glycans to produce complex glycans.[23,24] The addition of dibenzocyclooctyne (DBCO) coupled to Alexa Fluor 488 allowed the visualization of the incorporated modified sugars by means of Cu(I)-free "click chemistry."[24] Visualization of the samples by means of confocal imaging revealed the presence of newly modified sugars in dendrites that often showed a punctate distribution resembling that of GSs (Figure 2H). Accordingly, colocalization analysis confirmed that newly glycosylated proteins are enriched in GSs and, in fact, that ~50% of GSs are positive for each modified sugar (Figure 2I). Thus, *de novo* glycosylation is taking place at GSs, and GSs carry out complex glycosylation, as shown by the enrichment in Ac_4ManNAz that gets incorporated in sialic acid moieties (Figures 2H and 2I). Moreover, the distribution of the different sugars among GSs suggests that their glycosylation capabilities might be segregated and that, in this sense, functionally distinct GS might exist.

Polysialylation of NCAM essentially requires GSs in distal dendrites

An open question in the field, driven in part by the lack of evidence supporting the presence of functional Golgi membranes in dendrites, is whether locally secreted proteins may traffic through alternative routes to the plasma membrane.[2] In fact, core-glycosylated proteins have been shown to be unexpectedly abundant at the neuronal surface, suggesting that they have reached the plasma membrane without passing through Golgi.[8] Since GSs in dendrites have Golgi characteristics (Figures 1A and 1B) and carry out complex glycosylation (Figures 2H and 2I), we next asked whether complex glycosylation of synaptic transmembrane proteins is indeed a major function of this organelle in dendrites.

We have shown previously that the neural cell adhesion molecule NCAM is present at GSs.[13] NCAM is a transmembrane adhesion molecule that plays an important role in neuronal processes such as neurotransmission, synaptic plasticity, and memory formation.[26,27] This role is intimately linked to addition of polysialic acid (PolySia), a process called polysialylation.[28,29] Based on the finding that sialylated glycans are very prominent at GSs (Figures 2A, 2B, 2H, and 2I), and since NCAM is by far the most abundant substrate for polysialylation in neurons,[30] we reasoned that locally secreted NCAM will be glycosylated at GSs. In support of this hypothesis, we found that dendritic expression of St8SiaII, one of the two polysialyltransferases acting on NCAM, fused to GFP is highly enriched in GSs (Figures 2J and 2K). Of note, a catalytically inactive version of the enzyme was used in this experiment to maintain endogenous levels of PolySia while preserving the correct targeting of the enzyme in the cell. To further address whether NCAM may become polysialylated at GSs, we first assessed whether locally secreted NCAM traffics through GSs by taking advantage of the retention using selective hooks (RUSH) system that enables the controlled and

Figure 2. *De novo* complex glycosylation takes place at GSs in dendrites

(A) Representative images of primary neurons expressing pGolt-mCherry treated with biotinylated lectins. Concanavalin A (ConA) binds to core-glycosylated proteins, *wheat germ agglutinin* (WGA) binds to N-glycosylated proteins, and O-glycosylated proteins are detected with *helix pomatia lectin* (HPL). Visualization of lectins is achieved by incubation with Streptavidin-647. Scale bar is 5 μm.

(B) Percentage of GSs positive for each lectin (ConA, WGA, HPL) from the experiment in (A) ($n \geq 18$ dendrites from ≥ 6 cells from 2 independent primary cultures per lectin).

(C) Representative images from the CA1 somatic layer (top row) and stratum radiatum (bottom row) of mGolt brains treated with ConA to detect core-glycosylated proteins. Scale bars are 10 and 2 μm (inset).

(D) Percentage of GSs positive for ConA from the experiment in (C). Bars represent mean ± SEM (n = 16 from 2 littermate animals).

(E) Representative images of dendrites from neurons treated with 0.5 or 1.25 μM tunicamycin or DMSO as control and subsequently labeled with ConA. Scale bar is 5 μm.

(F) Quantification of ConA fluorescence intensity from (E) normalized to control (n = 29 dendrites from 2 independent primary cultures; one-way ANOVA with Bonferroni's multiple comparison test, ***$p < 0.001$; ns $p > 0.05$).

(G) Cartoon depicting the principle of the protocol used to detect *de novo* glycosylated proteins.

(H) Representative images of primary hippocampal neurons expressing pGolt-mCherry and treated with GlcNAz, ManNAz, or GalNAz followed by DBCO-488 for detecting N-glycans, sialic acid residues, and O-glycans, respectively. Scale bar is 5 μm.

(I) Percentage of GSs positive for each modified sugar from (H) (GlcNAz n = 21; ManNAz n = 17; GalNAz n = 23; from three independent cultures).

(J) Representative images of a primary hippocampal neuron expressing St8SiaII-GFP and pGolt-mCherry. Scale bar is 10 μm.

(K) Percentage of GSs positive for St8SiaII-GFP from (J) (n = 11 cells from 3 independent cultures).

(L) Schematic illustration of the principle of the RUSH system[22] used in (M) and (N). See Figures S2A–S2C.

(M) Representative images of primary neurons expressing pGolt-mCherry, Streptavidin-KDEL and GFP-SBP-NCAM at the time of biotin addition (0 min) and 60 min later. Scale bar is 10 μm. See also Figures S2A–S2C.

(N) Quantification the percentage of GSs enriched for GFP-SBP-NCAM from the experiment in (M) (n = 16 cells per group, three independent experiments; unpaired t test, ***$p > 0.0001$). See also Figures S2A–S2C.

synchronous release of tagged secretory cargo from the ER upon addition of biotin (Figure 2L).[22,31] Accordingly, we generated an expression vector containing NCAM fused to the streptavidin-binding peptide, a hemagglutinin (HA) tag, and GFP (GFP-SBP-NCAM, Figure 2L) and used the ER hook fused to the core streptavidin to ensure the retention of GFP-SBP-NCAM in the ER (Figure 2L). We tested its efficiency first in HEK293T cells where we could confirm that upon biotin addition, GFP-SBP-NCAM is released from the ER and subsequently localizes in the Golgi apparatus labeled by pGolt-mCherry (Figure S2A). The same approach in neurons demonstrated that GFP-SBP-NCAM is able to reach the plasma membrane, as evidenced by surface labeling using an anti-HA antibody, and where we found steady-state levels 2 h following biotin addition (Figures S2B and S2C). Half-maximal surface expression was reached 60 min after release (Figure S2C). In agreement with its retention in the ER, expression of GFP-SBP-NCAM in primary neurons was found to be homogeneously distributed along dendrites at the time of biotin application (Figures 2M and 2N). This distribution changed significantly 60 min after biotin application, when GFP-SBP-NCAM exhibited a punctate distribution (Figure 2M). Quantitative analysis revealed that >60% of analyzed GSs were enriched for GFP-SBP-NCAM at this time point (Figure 2N), which roughly matches with the number of GSs that are capable of *de novo* polysialylation (Figures 2H and 2I). Thus, NCAM that locally buds off from the dendritic ER passes through GSs, where it likely acquires polysialylation, and this appears to be a major function of a large number of GSs.

Loss of Calneuron-1 expression reduces GS density in distal dendrites

The study of cellular implications of local polysialylation of NCAM at GSs would benefit from a loss-of-function approach. Calneuron-1 and -2 are the two members of a subfamily of transmembrane CaM-like neuronal Ca^{2+}-binding proteins.[32] Calneurons are prominently located at the TGN and negatively control TGN-to-PM trafficking in a Ca^{2+}-dependent manner by inhibiting phosphatidylinositol 4-OH kinase III β (PI-4KIIIβ) and the production of PI-4 phosphate (PIP) (Figure S3A).[32] In consequence, the budding of vesicles from the TGN is attenuated, and calneurons thereby establish a Ca^{2+} threshold for activation of the enzyme and to retain membrane at the TGN (Figure S3A).[33] Calneuron-1 is, in contrast to Calneuron-2, abundantly expressed in pyramidal neurons of the CA1 region of the hippocampus,[34] and it is present at GSs.[13] We therefore reasoned that Calneuron-1 might also regulate local trafficking of secretory cargo through GSs in hippocampal dendrites.

To follow up on this notion, we generated a Calneuron-1-deficient transgenic mouse by removing the essential exon 2. This induces a frameshift in the major transcript that results in the elimination of *caln1* gene expression (Figure S3B). Analysis of Calneuron-1 levels by western blot analysis demonstrated that the protein is indeed absent from hippocampal and cerebellar samples of knockout (KO) animals (Figure S3B). Removal of the *caln1* gene did not result in gross alterations of structure of the hippocampus and cerebellum, as visualized by Nissl staining, compared with wild-type (WT) animals (Figures S3C and S3D). A more detailed analysis of the CA1 strata also revealed no major differences in the thickness of different layers (Figures S3E–S3H).

We then next assessed whether the absence of Calneuron-1 might result in an altered Golgi structure and neuronal morphology of pyramidal cells of the CA1 region. Immunostaining of cryosections from WT and KO animals with an antibody directed against the Golgi marker Giantin did not reveal major changes in the morphology of the somatic Golgi between genotypes (Figure 3A). A mild non-significant reduction was found in the length of the Golgi in neurons lacking Calneuron-1 (Figure 3B) that is largely due to the reduced number of neurons endowed with an extended Golgi (Figure 3C). Similarly, a reduction in Golgi length was found in primary hippocampal neurons of *caln1* KO mice that were stained with antibodies directed against the *cis*- and medial-Golgi marker GM130 and the *trans*-Golgi marker Syntaxin-6 (Figures 3D–3F).

In order to analyze whether the lack of Calneuron-1 might have an impact on GSs, we next generated double transgenic animals by crossing mice from the mGolt line with *caln1* KO mice, and we quantified the density of GSs in dendrites of the stratum radiatum proximal (SRP) and distal (SRD) as well as in the SLM, a stratum that contains the most distally located dendrites of CA1 pyramidal neurons (see scheme in Figure 3G). Importantly, we found a gradual decrease in GS abundance toward more distal dendrites, with respect to the cell soma of neurons from *caln1* KO brains, that is statistically significant in the SLM (Figures 3G–3I).

caln1 KO mice exhibit deficits in polysialylation of NCAM in distal dendrites

We next hypothesized that if GSs are implicated in the polysialylation of locally secreted NCAM, PSA-NCAM levels should be reduced in dendrites where GSs are significantly less abundant. To address this question, we labeled endogenous PSA-NCAM in dendrites of the SLM in WT and *caln1* KO brains using an antibody specifically directed against PolySia moieties made up of >10 sialic acid residues. In accordance with published work, sections from WT animals exhibited a steady increase of PSA-NCAM fluorescence intensity in dendrites from the SRP toward the SLM that correlated with an increase in NCAM immunofluorescence (Figures 4A and 4B).[35] A similar distribution of NCAM levels was seen in brain sections from *caln1* KO mice (Figures 4B and 4E). However, unlike in WT brains, PSA-NCAM levels were significantly decreased in dendrites of the SRD and SLM in CA1 pyramidal neurons lacking Calneuron-1 (Figures 4A and 4C–4E). This reduction was correlated with the reduction of the number of GSs (Figures 3G and 3H). Since quantification of hippocampal mRNA levels by qPCR demonstrated that levels of NCAM as well as the polysialyltransferases involved in NCAM polysialylation St8SiaII and St8SiaIV are not affected in KO animals compared WT (Figure 4F), these data strongly suggest that reduced PSA-NCAM levels found in distal dendrites of the SLM are likely due to the decreased number of GSs.

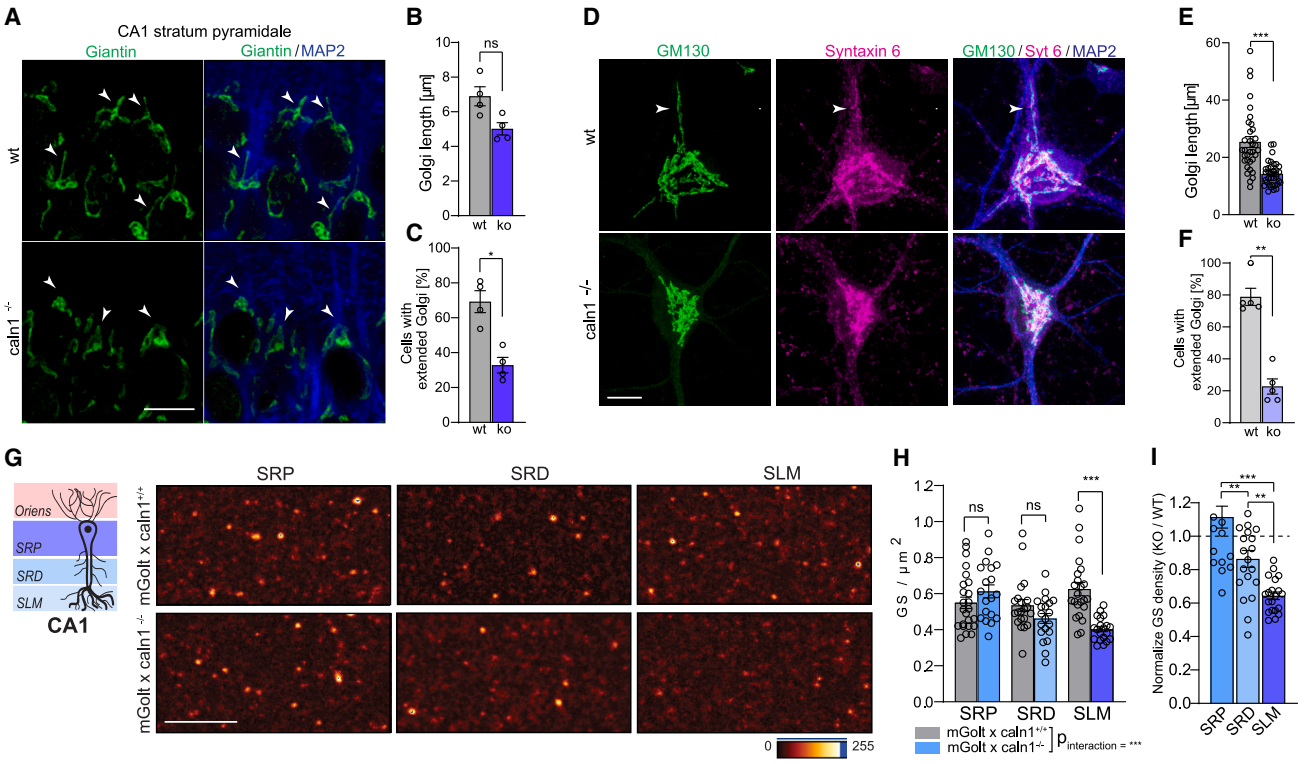

Figure 3. Loss of Calneuron-1 expression reduces GS density in distal dendrites

(A) Representative images of the CA1 stratum pyramidale from cryosections of *caln1* KO and WT mice stained against the Golgi marker Giantin and MAP2. Arrows point to extended Golgi. Scale bar is 10 µm. See also Figures S3A–S3D.

(B) Quantification of Golgi length from (A) (n = 4 slices from 2 litter pairs; Mann-Whitney U test; ns $p > 0.05$). See also Figures S3A–S3D.

(C) Percentage of cells with extended Golgi from (A) (n = 4 slices from 2 litter pairs; Mann-Whitney U test; *$p < 0.05$). See also Figures S3A–S3D.

(D) Hippocampal primary neurons from *caln1* KO and WT mice stained with antibodies against GM130, Syntaxin 6, and MAP2. Arrows indicate extended Golgi. Scale bar is 10 µm.

(E) Quantification of the Golgi length from (D) (n = 36 cells from 3 independent cultures; Mann-Whitney U test; ***$p < 0.001$).

(F) Percentage of neurons with extended Golgi from (D) (n = 4 coverslips from 3 independent cultures; Mann-Whitney U test; **$p < 0.01$)

(G) Left, scheme depicting the different strata in which CA1 pyramidal neurons are organized. Right, representative images from the SRP, SRD, and SLM in the CA1 region of double transgenic animals expressing pGolt under *caln1* KO and WT backgrounds. Scale bar is 5 µm. See also Figures S3F–S3H.

(H) Quantification of the density of GSs per strata from the experiment in (H) (circles represent images acquired from 4 littermates per genotype; two-way ANOVA; ns $p > 0.05$, ***$p < 0.001$). See also Figures S3F–S3H.

(I) Bar graph showing GS density in each strata of mGolt × *caln1*$^{-/-}$ animals normalized to GS density in the corresponding strata of mGolt × *caln1*$^{+/+}$ animals (one-way ANOVA with Tukey's multiple comparison test; **$p < 0.01$; ***$p < 0.0001$). See also Figures S3F–S3H.

Synapse density is reduced in distal dendrites following Calneuron-1 protein knockdown or gene KO

PSA-NCAM has a documented role in synaptic plasticity as well as synapse formation and stability.[30,36,37] We next assessed whether the reduced number of GS in *caln1* KO mice has an impact on neuronal morphology and synapse density in the SLM. To this end, we took advantage of the Cre-LoxP system to sparsely express GFP in pyramidal cells of the CA1 region of the hippocampus. Accordingly, we delivered two viruses (AAV9-EF1α-LoxP-EGFP-LoxP and AAV9-CaMKII-Cre) to the CA1 hippocampal region of WT and KO littermates by means of a transcranial injection (Figure 5A). High-resolution scanning confocal microscopy revealed sparse labeling of pyramidal neurons with EGFP and that the overall neuronal morphology did not appear to be affected by the absence of Calneuron-1 (Figure 5B). Quantification of spine density, however, performed from different dendritic segments acquired in the SRD and the SLM regions (Figures 5B and 5C) revealed a reduction in spine density toward distal dendrites in the KO mice that becomes statistically significant in dendritic segments of the SLM but not in other strata (Figure 5D).

To exclude the effects of gene KO on early neuronal development and to corroborate these findings, we tested the effect of a short hairpin RNA-mediated pan Calneuron protein knockdown (KD) on neuronal morphology in hippocampal primary neurons.[33] Like in KO mice, reduced Calneuron levels did not result in major changes in the length of the somatic Golgi (Figures S4A and S4B) or the percentage of cells endowed with extended Golgi (Figure S4C). However, these neurons showed a significant reduction in branching of distal dendrites as revealed by Sholl analysis (Figures 5E and 5F) and a

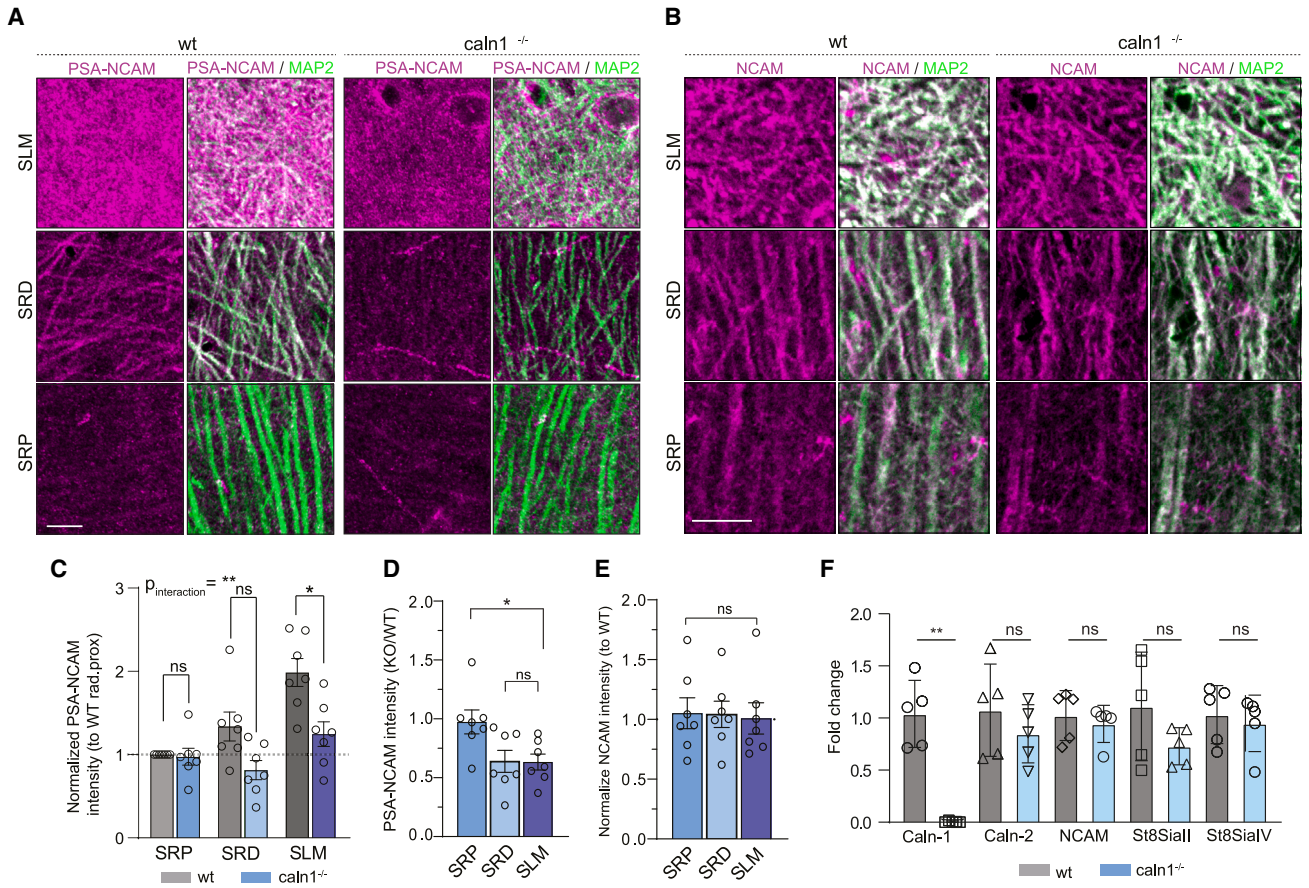

Figure 4. Polysialylation of NCAM essentially requires GSs in distal dendrites

(A) Representative images from the different strata in the CA1 region of *caln1* KO and WT brains stained with PSA-NCAM and MAP2. Scale bar is 10 μm.

(B) Representative images from the different strata in the CA1 region of *caln1* KO and WT brains stained with NCAM and MAP2. Scale bar is 10 μm.

(C) Quantification PSA-NCAM intensity in MAP2-positive regions from the experiment in (A) normalized to WT SRP (n = 7 animals per genotype; two-way ANOVA repeated measures with Sidak's multiple comparison test, ns $p > 0.05$; *$p < 0.05$; **$p < 0.01$).

(D) PSA-NCAM fluorescence intensity from the KO animals relative to WT and normalized to data from SRP (n = 7 animals per genotype; Kruskal-Wallis test, *$p < 0.05$; ns $p > 0.05$).

(E) NCAM fluorescence intensity from KO animals relative to WT and normalized to data from SRP (n = 7 animals per genotype; Kruskal-Wallis test, ns $p > 0.05$).

(F) qPCR performed from hippocampi. The expression of Calneuron-1, Calneuron-2, NCAM, and its main polysialyltransferases, ST8SiaII and ST8SiaIV, were measured (n = 5 animals per genotype; Mann-Whitney test, ns $p > 0.05$; **$p < 0.01$).

significant decrease in the number of excitatory synapses that was most prominent in tertiary dendrites (Figures 5G and 5H).

Impaired long-term synaptic plasticity in distal dendrites of temporoammonic connections to CA1-SLM in *caln1* KO mice

PSA-NCAM is known to regulate long-term synaptic plasticity.[37,38] In order to study the implications of reduced GS and PSA-NCAM levels in distal dendrites of the SLM for neurotransmission and synaptic plasticity, we performed electrophysiological recordings. To specifically asses distal synaptic contacts of the SLM, we stimulated the temporoammonic (TA) pathway to CA1-SLM[39,40] and compared the properties of evoked responses with those obtained upon stimulation of the Schaffer collateral pathway (SC-CA1), which also contacts CA1 pyramidal neurons but at dendrites located at the stratum radiatum (Figure 6A). Initial analysis of the amplitude of field excitatory postsynaptic potentials (fEPSPs) and paired-pulse facilitation revealed a significant impairment of the fEPSP amplitude in *caln1* KO mice compared with the WT animals, while paired-pulse facilitation remained unaffected (Figures S5A–S5D). Accordingly, similar reductions in the fEPSP amplitude by 40% were obtained for both types of responses recorded in the SC-CA1 to proximal dendrites in the stratum radiatum (Figures S5A and S5B) as well as the TA-CA1 pathway to distal dendrites in the SLM (Figures S5C and S5D). Considering no changes in presynaptic paired-pulse facilitation, impaired basal synaptic transmission is likely to reflect a loss of the number of spines and excitatory synapses rather than a reduction in the efficacy of presynaptic glutamate release.

Next, we induced long-term potentiation (LTP) in acute slices from WT and KO animals using a high-frequency stimulation

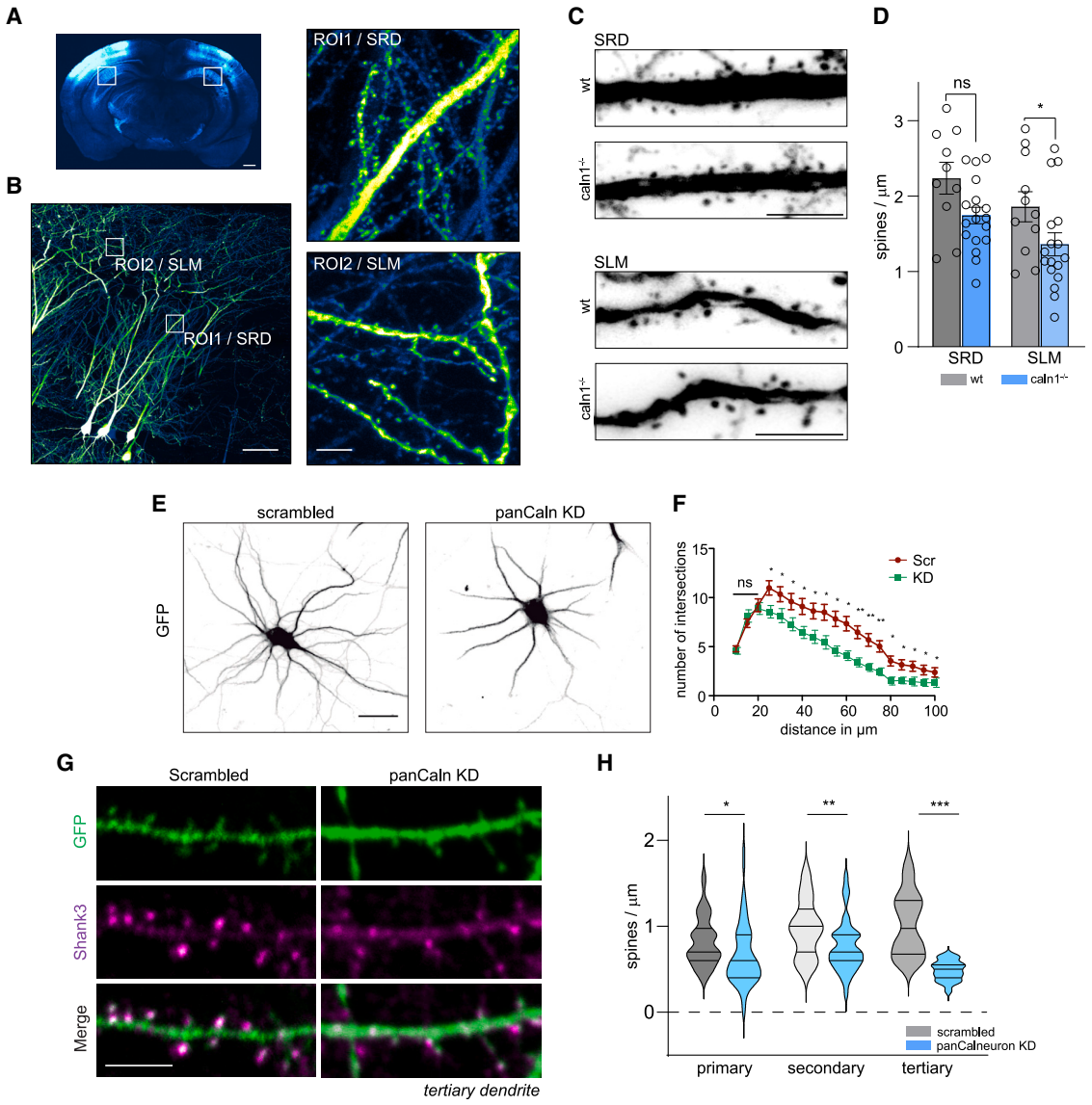

Figure 5. Synapse density is reduced in dendrites of the SLM in *caln1* KO mice

(A) GFP fluorescence in a coronal section obtained from a mouse that underwent intracranial virus delivery. Boxes indicate analyzed regions. Scale bar is 500 µm.

(B) Representative images of pyramidal neurons of the CA1 expressing GFP and example analyzed areas of the SRD and SLM. Scale bars are 50 and 5 µm (zoomed-in regions).

(C) Representative dendritic segments obtained from the SRD and SLM of 14-week-old *caln1* WT and KO animals injected with AAV-Cre and AAV-GFP$^{lx/lx}$. Scale bar is 5 µm.

(D) Quantification of spine density from (A)–(C) (WT_{SRD} n = 10; KO_{SRD} n = 18; WT_{SLM} n = 11; KO_{SLM} n = 17; N = 3 animals per genotype; unpaired t test, ns $p > 0.05$; *$p < 0.05$).

(E) Representative images of days *in vitro* (DIV) 8 primary neurons transfected with the pan CalnKD or a scrambled control plasmid at DIV3. Scale bar is 10 µm. See also Figures S4A–S4C.

(F) Sholl analysis of neurons from the experiment in (E) (scrambled n = 32; KD n = 27 from 3 independent cultures; Student's t test for each time point; ns $p > 0.05$; *$p < 0.05$; **$p < 0.01$; ***$p < 0.001$). See also Figures S4A–S4C.

(G) Representative images of tertiary dendrites from hippocampal primary neurons expressing pan CalnKD or a scrambled control construct at DIV 9 and fixed at DIV 14. Cells were stained with an antibody against the synaptic marker Shank3. Scale bar is 10 µm. See also Figures S4A–S4C.

(H) Synapse quantification from (G). The number of synapses was counted in primary, secondary, and tertiary dendrites (n = 3 experiments; scrambled [Scr] n = 24 KD n = 19; Kolmogorov-Smirnov test for primary and secondary dendrite groups; unpaired t test for the tertiary dendrite group). See also Figures S4A–S4C.

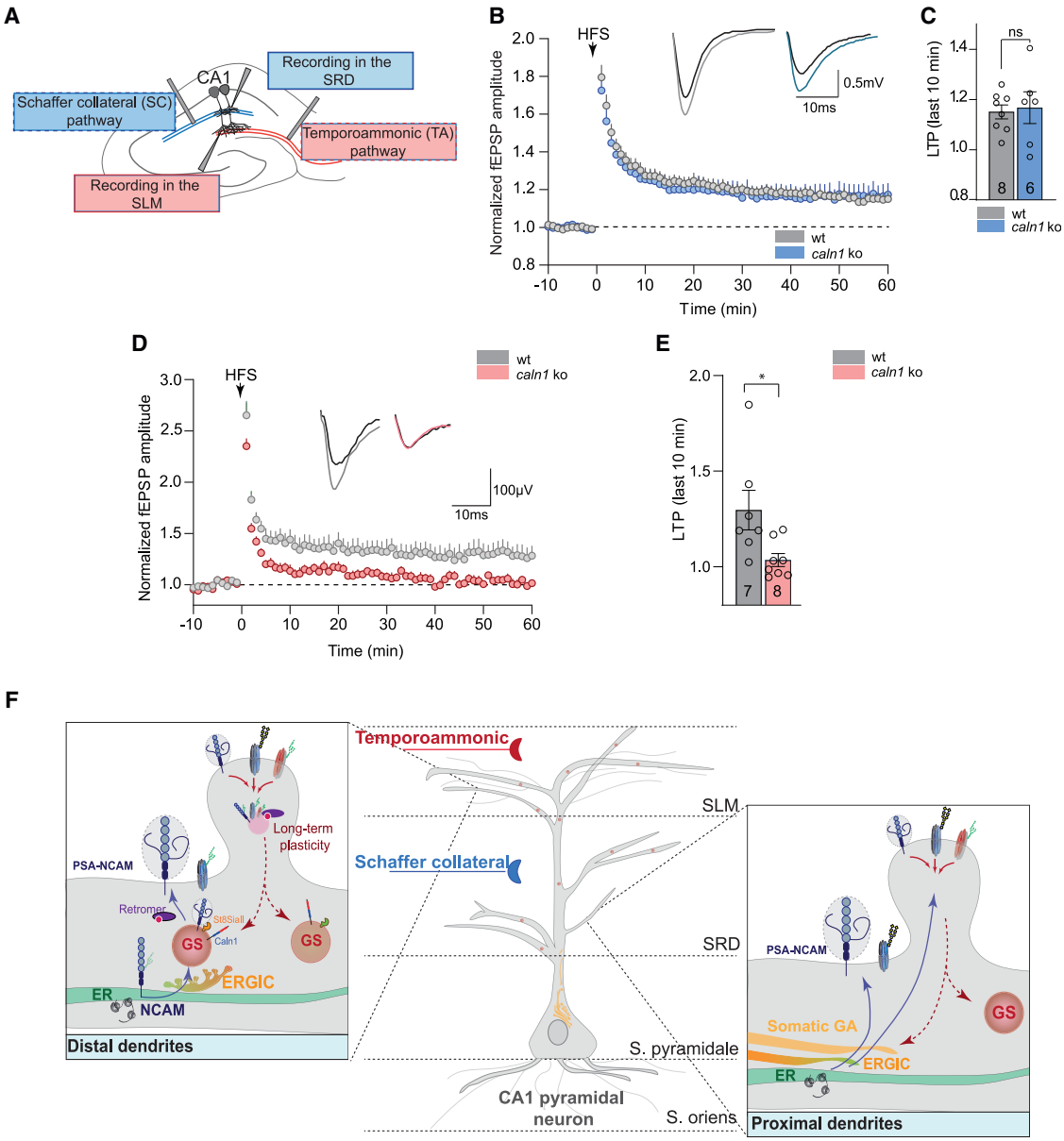

Figure 6. Long-term potentiation is impaired in dendrites of the SLM in *caln1* KO mice

(A) Cartoon depicting the different pathway used to differentially stimulate distal dendrites of the SLM and more proximal dendrites of the SRD of pyramidal neurons in the CA1 for the experiment in (B)–(E). See also Figures S5A–S5E.

(B) Average fEPSP amplitudes upon long-term potentiation (LTP) induction in the Schaffer collateral-CA1 pathway (WT n = 8; KO n = 6). See also Figures S5A and S5B.

(C) Averaged fEPSP amplitudes obtained during the last 10 min of (B) (WT n = 8; KO n = 6; Mann-Whitey test; ns $p > 0.05$). See also Figures S5A and S5B.

(D) Average fEPSP amplitudes upon LTP induction in the temporammonic-CA1 path (WT n = ; KO n = 8; KO+PolySia = 6). See also Figures S5C–S5E.

(E) Averaged fEPSP amplitudes obtained during the last 10 min of (D) (WT n = ; KO n = 8; KO+PolySia = 6; Kruskal-Wallis test with Dunn's correction; *$p < 0.05$). See also Figures S5C–S5E.

(F) Summary cartoon. In distal dendrites of the SLM receiving input from the temporoammonica pathway, GSs play a fundamental role in the polysialylation of locally secreted NCAM, which is required for induction and maintenance of LTP exclusively in distal synapses. The glycosylation function of GSs at distal regions might not be restricted to NCAM and to forward trafficking, and GSs may as well receive cargo from the plasma membrane via retromer. The need for glycosylation of proximal dendrites of the stratum radiatum that receive input from the Schaffer collateral pathway are also more likely to be fulfilled by the somatic Golgi, which is localized in a closer proximity.

protocol. Recordings from the SC-CA1 pathway revealed no deficits in the maintenance of LTP in KO neurons when compared with WT (Figures 6B and 6C). However, LTP induction in the TA-CA1 pathway to dendrites in the SLM was significantly impaired in KO animals (Figures 6D and 6E). Importantly, this deficiency is not due to a differential expression of NMDA receptors since the relative contribution of NMDAR to TA-CA1 fEPSP in the SLM is similar between WT and KO animals (Figure S5E), indicating that PolySia reduction does not affect NMDAR expression, in line with results obtained upon enzymatic PolySia removal.[41] Collectively, these data indicate that loss of Calneuron-1 causes a selective deficit in the expression of LTP at distal dendrites of the SLM in CA1 neurons, which is very likely due to a deficiency in PSA-NCAM and that, in turn, might be caused by a reduced number of GSs in these dendrites.

DISCUSSION

In light of the remoteness of synaptic contact sites relative to protein synthesis machinery in the cell body, local secretory organelles have the significant advantage of timely and possibly on-demand supply of membrane proteins.[2] At present, however, it is still unclear how local secretory organelles are involved in the processing of synaptic membrane proteins in dendrites and, in particular, whether and how maturation of locally secreted synaptic transmembrane proteins affects neurotransmission and plasticity.[2] Here, we provide compelling evidence that dendritic GS membranes resemble features of the TGN and that they provide local mature glycosylation in those dendritic segments where demands for protein maturation are difficult to be fulfilled by the function of the somatic Golgi. Accordingly, ultrastructural, biochemical, and functional data indicate that GSs represent a widespread structurally and functionally simplified form of Golgi that serve as glycosylation platforms for synaptic membrane proteins.

Different types of glycosylation take place at GSs

Collectively, our data suggest the existence of functionally different GS populations capable of carrying out different types of glycosylation. This assumption is based on metabolic labeling experiments where we never found more than 50% of GSs positive for each of the analyzed sugars (Figures 2H and 2I). Since protein glycosylation requires the activity of several enzymes acting in a sequential manner,[17,18] different GS populations would represent a functional advantage in order to achieve fast and efficient glycosylation. Taking into consideration the simplified structure of GSs lacking cisternae, it is likely that glycosylation enzymes involved in the same glycosylation routes are present within the same GS microcompartment, whereas unrelated enzymes might be absent. The presence of different GS populations would also necessitate distinct microsecretory routes that each post-ER carrier would have to take based on the molecular identity of cargo.[10] How this is organized locally and how synaptic activity may regulate these processes need to be studied in future work. Of note in this regard, data from a recent study indicate that proteins that are locally processed in dendritic ER networks are widely dispersed before surface insertion.[10] It will be interesting to investigate whether this dispersion might also imply trafficking through GSs or whether cargo leaving GSs gets inserted in nearby synapses.

GSs are essential for maintenance of PSA-NCAM levels in distal dendrites

An intriguing question that comes along with these findings is which factors might determine the choice of microsecretory route for trafficking of a given cargo to the plasma membrane. Previous work has shown that distinct secretory routes for different proteins exist that include trafficking through Golgi as well as Golgi bypass.[7,8,10,12,13] Sorting of newly synthesized proteins to the plasma membrane that bypasses the Golgi is not uncommon, and Golgi-independent trafficking routes that are sorted non-polarly to the plasma membrane usually serve housekeeping cell functions. Current evidence suggests that, predominantly under basal conditions, proteins lacking mature glycosylation, including those with a direct impact on synaptic transmission like synaptic adhesion molecules and neurotransmitter receptors, get inserted to the surface of dendritic membranes, suggesting a bypass of Golgi.[8]

The present study demonstrates that polysialylation of NCAM at GSs determines PSA-NCAM levels and is essential for the expression of LTP in remote synapses of the SLM in CA1 neurons. PSA is a linear homopolymer of sialic acid whose length varies between a few and more than a hundred monomers.[42] NCAM is the main carrier of PSA in the brain, and St8SiaII, one of the two main responsible enzymes for NCAM polysialylation, localizes at GSs (Figures 2J and 2K).[27] Considering the relative simplicity of GSs, one has to assume that their capacity for local glycosylation is limited, and it is thus likely that only a subset of proteins will be glycosylated in GSs. Here, NCAM appears to be one, if not the most prominent, example. Thus, GSs could serve as glycosylation sites for immature proteins inserted at the neuronal surface whose function under certain activity conditions might require their full maturation. This would rapidly contribute to changes in the functional properties as well as the lifetime of proteins and support relatively fast changes in synaptic transmission.

Along these lines, neuronal activity increases synaptic PSA-NCAM levels that are required for the induction of long-term plasticity in synapses of CA1 neurons.[30,43–45] Moreover, a recent study reported changes in the glycosylation pattern of surface proteins that were linked to the biogenesis of Golgi fragments in response to nicotine stimulation for 17 h.[46] Interestingly, mature sialylated residues were most prominently regulated under these conditions.[46] It will be therefore interesting to address in future work whether induction of LTP will result in an increased number of GSs and thereby increased PSA-NCAM levels. In experiments performed with primary neurons, however, a general enhancement of neuronal activity as such did not cause an instantaneous effect on the number of GSs (data not shown).

Cellular implications of GSs in dendrites

We were able to address the functional significance and cellular implications of GS glycosylation in distal dendrites based on a loss-of-function approach provided by the fact that neurons lacking Calneuron-1 have a significant decrease in GS abundance that is most prominent in distal dendrites (Figures 3G

and 3H). This is correlated with impaired LTP of synapses of the TA pathway located at distal dendritic branches of the SLM and a reduced synapse number. Since PSA-NCAM has an important role in neuronal development and synaptic plasticity,[47] the mild decrease in spine density in SLM dendrites (Figure 5D) might be caused by reduced PSA-NCAM levels found in KO neurons, and this, in turn, might cause the defects in LTP found in *caln1* KO neurons. Thus, we hypothesize that interference with polysialylation of NCAM could rescue the observed KO phenotype.

Limitations of the study

An important aspect, which we could not take into consideration in our study, is the potential diversity of GSs in terms of molecular composition and function. Knowledge about the molecular composition of GSs is still very limited, and this hampers the identification of endogenous marker proteins that would be helpful to study GSs and to define potential GS subpopulations in future work.

STAR★METHODS

Detailed methods are provided in the online version of this paper and include the following:

- KEY RESOURCES TABLE
- RESOURCE AVAILABILITY
  - Lead contact
  - Materials availability
  - Data and code availability
- EXPERIMENTAL MODEL AND STUDY PARTICIPANT DETAILS
  - Rat primary hippocampal culture
  - Mouse hippocampal primary cultures
  - Cell lines
- METHOD DETAILS
  - Generation of transgenic mice
  - Transfection
  - NCAM release with the RUSH system
  - Live-labeling, immunostaining, and imaging
  - Electron microscopy
  - Biochemistry
  - SDS-PAGE
  - Immunoblotting
  - Southern blot
  - qPCR
  - Electrophysiology
  - Analysis of basal transmission and plasticity
  - Spine count in CA1 pyramidal neurons
- QUANTIFICATION AND STATISTICAL ANALYSIS

SUPPLEMENTAL INFORMATION

Supplemental information can be found online at https://doi.org/10.1016/j.celrep.2023.112692.

ACKNOWLEDGMENTS

The authors gratefully acknowledge the professional technical assistance of C. Borutzi, M. Marunde, and I. Herbert; Dr. A.V. Failla for help with image acquisition and analysis; and Prof. Dr. E.D. Gundelfinger for valuable discussion. We would like to thank Dr. Ingke Braren from the UKE Vector Facility and Dr. Julie C. Johnston, University of Pennsylvania, USA, for AAV9 virus production, and the Transgenic Facility at the ZMNH/UKE for their helpful support. We would also like to thank Prof. Dr. Martin Spiess for sharing the CIMPR and CDMPR expression vectors. This work is supported by grants from the Deutsche Forschungsgemeinschaft (DFG) (KR1879/FOR2419; FOR5228 RP6; CRC 1436 TPA02, A04, A05 and Z01). Microscopes used to acquire data in this study were acquired with DFG funds (INST 152/933-1).

AUTHOR CONTRIBUTIONS

M.A.-A., M.B., and M.R.K. designed the study; M.A.-A., M.B., J.L., K.K., H.M., and M.S., conducted the experiments; M.A.-A., M.B., J.L., K.K., H.M., S.H.-U., A.D., and M.R.K. analyzed the data; S.H.-U. and A.O. provided methods and tools; M.A.-A. curated data and prepared figures; M.A.-A. and M.R.K. wrote the paper; and all authors commented and revised the manuscript.

DECLARATION OF INTERESTS

The authors declare no competing interests.

Received: December 22, 2022
Revised: April 28, 2023
Accepted: June 8, 2023
Published: June 24, 2023

REFERENCES

1. Dieterich, D.C., and Kreutz, M.R. (2016). Proteomics of the Synapse–A Quantitative Approach to Neuronal Plasticity. Mol. Cell. Proteomics *15*, 368–381. https://doi.org/10.1074/mcp.R115.051482.
2. Grochowska, K.M., Andres-Alonso, M., Karpova, A., and Kreutz, M.R. (2022). The needs of a synapse-How local organelles serve synaptic proteostasis. EMBO J. *41*, e110057. https://doi.org/10.15252/embj.2021110057.
3. Rosenberg, T., Gal-Ben-Ari, S., Dieterich, D.C., Kreutz, M.R., Ziv, N.E., Gundelfinger, E.D., and Rosenblum, K. (2014). The roles of protein expression in synaptic plasticity and memory consolidation. Front. Mol. Neurosci. *7*, 86. https://doi.org/10.3389/fnmol.2014.00086.
4. Hanus, C., and Ehlers, M.D. (2016). Specialization of biosynthetic membrane trafficking for neuronal form and function. Curr. Opin. Neurobiol. *39*, 8–16. https://doi.org/10.1016/j.conb.2016.03.004.
5. Kennedy, M.J., and Hanus, C. (2019). Architecture and Dynamics of the Neuronal Secretory Network. Annu. Rev. Cell Dev. Biol. *35*, 543–566. https://doi.org/10.1146/annurev-cellbio-100818-125418.
6. Wu, Y., Whiteus, C., Xu, C.S., Hayworth, K.J., Weinberg, R.J., Hess, H.F., and De Camilli, P. (2017). Contacts between the endoplasmic reticulum and other membranes in neurons. Proc. Natl. Acad. Sci. USA *114*, E4859–E4867. https://doi.org/10.1073/pnas.1701078114.
7. Bowen, A.B., Bourke, A.M., Hiester, B.G., Hanus, C., and Kennedy, M.J. (2017). Golgi-independent secretory trafficking through recycling endosomes in neuronal dendrites and spines. Elife *6*, e27362. https://doi.org/10.7554/eLife.27362.
8. Hanus, C., Geptin, H., Tushev, G., Garg, S., Alvarez-Castelao, B., Sambandan, S., Kochen, L., Hafner, A.S., Langer, J.D., and Schuman, E.M. (2016). Unconventional secretory processing diversifies neuronal ion channel properties. Elife *5*, e20609. https://doi.org/10.7554/eLife.20609.
9. Hanus, C., and Ehlers, M.D. (2008). Secretory outposts for the local processing of membrane cargo in neuronal dendrites. Traffic *9*, 1437–1445. https://doi.org/10.1111/j.1600-0854.2008.00775.x.
10. Bourke, A.M., Schwartz, S.L., Bowen, A.B., Kleinjan, M.S., Winborn, C.S., Kareemo, D.J., Gutnick, A., Schwarz, T.L., and Kennedy, M.J. (2021). zapERtrap: A light-regulated ER release system reveals unexpected

neuronal trafficking pathways. J. Cell Biol. *220*, e202103186. https://doi.org/10.1083/jcb.202103186.

11. Gu, Y., Chiu, S.L., Liu, B., Wu, P.H., Delannoy, M., Lin, D.T., Wirtz, D., and Huganir, R.L. (2016). Differential vesicular sorting of AMPA and GABAA receptors. Proc. Natl. Acad. Sci. USA *113*, E922–E931. https://doi.org/10.1073/pnas.1525726113.
12. Jeyifous, O., Waites, C.L., Specht, C.G., Fujisawa, S., Schubert, M., Lin, E.I., Marshall, J., Aoki, C., de Silva, T., Montgomery, J.M., et al. (2009). SAP97 and CASK mediate sorting of NMDA receptors through a previously unknown secretory pathway. Nat. Neurosci. *12*, 1011–1019. https://doi.org/10.1038/nn.2362.
13. Mikhaylova, M., Bera, S., Kobler, O., Frischknecht, R., and Kreutz, M.R. (2016). A Dendritic Golgi Satellite between ERGIC and Retromer. Cell Rep. *14*, 189–199. https://doi.org/10.1016/j.celrep.2015.12.024.
14. Braulke, T., and Bonifacino, J.S. (2009). Sorting of lysosomal proteins. Biochim. Biophys. Acta *1793*, 605–614. https://doi.org/10.1016/j.bbamcr.2008.10.016.
15. Saftig, P., and Klumperman, J. (2009). Lysosome biogenesis and lysosomal membrane proteins: trafficking meets function. Nat. Rev. Mol. Cell Biol. *10*, 623–635. https://doi.org/10.1038/nrm2745.
16. Klumperman, J. (2011). Architecture of the mammalian Golgi. Cold Spring Harb. Perspect. Biol. *3*, a005181. https://doi.org/10.1101/cshperspect.a005181.
17. Stanley, P. (2011). Golgi glycosylation. Cold Spring Harb. Perspect. Biol. *3*, a005199. https://doi.org/10.1101/cshperspect.a005199.
18. Zhang, X., and Wang, Y. (2016). Glycosylation Quality Control by the Golgi Structure. J. Mol. Biol. *428*, 3183–3193. https://doi.org/10.1016/j.jmb.2016.02.030.
19. Moremen, K.W., Tiemeyer, M., and Nairn, A.V. (2012). Vertebrate protein glycosylation: diversity, synthesis and function. Nat. Rev. Mol. Cell Biol. *13*, 448–462. https://doi.org/10.1038/nrm3383.
20. Bhavanandan, V.P., and Katlic, A.W. (1979). The interaction of wheat germ agglutinin with sialoglycoproteins. The role of sialic acid. J. Biol. Chem. *254*, 4000–4008.
21. Rambaruth, N.D.S., Greenwell, P., and Dwek, M.V. (2012). The lectin Helix pomatia agglutinin recognizes O-GlcNAc containing glycoproteins in human breast cancer. Glycobiology *22*, 839–848. https://doi.org/10.1093/glycob/cws051.
22. Boncompain, G., Divoux, S., Gareil, N., de Forges, H., Lescure, A., Latreche, L., Mercanti, V., Jollivet, F., Raposo, G., and Perez, F. (2012). Synchronization of secretory protein traffic in populations of cells. Nat. Methods *9*, 493–498. https://doi.org/10.1038/nmeth.1928.
23. Hayes, J.M., O'Hara, D.M., and Davey, G.P. (2022). Metabolic Labeling of Primary Neurons Using Carbohydrate Click Chemistry. Methods Mol. Biol. *2370*, 315–322. https://doi.org/10.1007/978-1-0716-1685-7_16.
24. Laughlin, S.T., and Bertozzi, C.R. (2007). Metabolic labeling of glycans with azido sugars and subsequent glycan-profiling and visualization via Staudinger ligation. Nat. Protoc. *2*, 2930–2944. https://doi.org/10.1038/nprot.2007.422.
25. Laughlin, S.T., and Bertozzi, C.R. (2009). Imaging the glycome. Proc. Natl. Acad. Sci. USA *106*, 12–17. https://doi.org/10.1073/pnas.0811481106.
26. Maness, P.F., and Schachner, M. (2007). Neural recognition molecules of the immunoglobulin superfamily: signaling transducers of axon guidance and neuronal migration. Nat. Neurosci. *10*, 19–26. https://doi.org/10.1038/nn1827.
27. Senkov, O., Tikhobrazova, O., and Dityatev, A. (2012). PSA-NCAM: synaptic functions mediated by its interactions with proteoglycans and glutamate receptors. Int. J. Biochem. Cell Biol. *44*, 591–595. https://doi.org/10.1016/j.biocel.2012.01.008.
28. Dityatev, A., Dityateva, G., Sytnyk, V., Delling, M., Toni, N., Nikonenko, I., Muller, D., and Schachner, M. (2004). Polysialylated neural cell adhesion molecule promotes remodeling and formation of hippocampal synapses. J. Neurosci. *24*, 9372–9382. https://doi.org/10.1523/JNEUROSCI.1702-04.2004.
29. Weinhold, B., Seidenfaden, R., Röckle, I., Mühlenhoff, M., Schertzinger, F., Conzelmann, S., Marth, J.D., Gerardy-Schahn, R., and Hildebrandt, H. (2005). Genetic ablation of polysialic acid causes severe neurodevelopmental defects rescued by deletion of the neural cell adhesion molecule. J. Biol. Chem. *280*, 42971–42977. https://doi.org/10.1074/jbc.M511097200.
30. Muller, D., Wang, C., Skibo, G., Toni, N., Cremer, H., Calaora, V., Rougon, G., and Kiss, J.Z. (1996). PSA-NCAM is required for activity-induced synaptic plasticity. Neuron *17*, 413–422. https://doi.org/10.1016/s0896-6273(00)80174-9.
31. Boncompain, G., and Perez, F. (2012). Synchronizing protein transport in the secretory pathway. Curr Protoc Cell Biol. Chapter *15*, cb1519s57, Unit 15 19. https://doi.org/10.1002/0471143030.
32. Mundhenk, J., Fusi, C., and Kreutz, M.R. (2019). Caldendrin and Calneurons-EF-Hand CaM-Like Calcium Sensors With Unique Features and Specialized Neuronal Functions. Front. Mol. Neurosci. *12*, 16. https://doi.org/10.3389/fnmol.2019.00016.
33. Mikhaylova, M., Reddy, P.P., Munsch, T., Landgraf, P., Suman, S.K., Smalla, K.H., Gundelfinger, E.D., Sharma, Y., and Kreutz, M.R. (2009). Calneurons provide a calcium threshold for trans-Golgi network to plasma membrane trafficking. Proc. Natl. Acad. Sci. USA *106*, 9093–9098. https://doi.org/10.1073/pnas.0903001106.
34. Hradsky, J., Bernstein, H.G., Marunde, M., Mikhaylova, M., and Kreutz, M.R. (2015). Alternative splicing, expression and cellular localization of Calneuron-1 in the rat and human brain. J. Histochem. Cytochem. *63*, 793–804. https://doi.org/10.1369/0022155415595841.
35. Pesarico, A.P., Bueno-Fernandez, C., Guirado, R., Gómez-Climent, M.Á., Curto, Y., Carceller, H., and Nacher, J. (2019). Chronic Stress Modulates Interneuronal Plasticity: Effects on PSA-NCAM and Perineuronal Nets in Cortical and Extracortical Regions. Front. Cell. Neurosci. *13*, 197. https://doi.org/10.3389/fncel.2019.00197.
36. Bonfanti, L., and Theodosis, D.T. (2009). Polysialic acid and activity-dependent synapse remodeling. Cell Adh. Migr. *3*, 43–50. https://doi.org/10.4161/cam.3.1.7258.
37. Senkov, O., Sun, M., Weinhold, B., Gerardy-Schahn, R., Schachner, M., and Dityatev, A. (2006). Polysialylated neural cell adhesion molecule is involved in induction of long-term potentiation and memory acquisition and consolidation in a fear-conditioning paradigm. J. Neurosci. *26*, 10888–109898. https://doi.org/10.1523/JNEUROSCI.0878-06.2006.
38. Kochlamazashvili, G., Senkov, O., Grebenyuk, S., Robinson, C., Xiao, M.F., Stummeyer, K., Gerardy-Schahn, R., Engel, A.K., Feig, L., Semyanov, A., et al. (2010). Neural cell adhesion molecule-associated polysialic acid regulates synaptic plasticity and learning by restraining the signaling through GluN2B-containing NMDA receptors. J. Neurosci. *30*, 4171–4183. https://doi.org/10.1523/JNEUROSCI.5806-09.2010.
39. Aksoy-Aksel, A., and Manahan-Vaughan, D. (2013). The temporoammonic input to the hippocampal CA1 region displays distinctly different synaptic plasticity compared to the Schaffer collateral input in vivo: significance for synaptic information processing. Front. Synaptic Neurosci. *5*, 5. https://doi.org/10.3389/fnsyn.2013.00005.
40. Remondes, M., and Schuman, E.M. (2003). Molecular mechanisms contributing to long-lasting synaptic plasticity at the temporoammonic-CA1 synapse. Learn. Mem. *10*, 247–252. https://doi.org/10.1101/lm.59103.
41. Varbanov, H., Jia, S., Kochlamazashvili, G., Bhattacharya, S., Buabeid, M.A., El Tabbal, M., Hayani, H., Stoyanov, S., Sun, W., Thiesler, H., et al. (2023). Rescue of synaptic and cognitive functions in polysialic acid-deficient mice and dementia models by short polysialic acid fragments. Neurobiol. Dis. *180*, 106079. https://doi.org/10.1016/j.nbd.2023.106079.
42. Rutishauser, U. (2008). Polysialic acid in the plasticity of the developing and adult vertebrate nervous system. Nat. Rev. Neurosci. *9*, 26–35. https://doi.org/10.1038/nrn2285.

43. Boll, I., Jensen, P., Schwämmle, V., and Larsen, M.R. (2020). Depolarization-dependent Induction of Site-specific Changes in Sialylation on N-linked Glycoproteins in Rat Nerve Terminals. Mol. Cell. Proteomics *19*, 1418–1435. https://doi.org/10.1074/mcp.RA119.001896.

44. Scott, H., and Panin, V.M. (2014). N-glycosylation in regulation of the nervous system. Adv. Neurobiol. *9*, 367–394. https://doi.org/10.1007/978-1-4939-1154-7_17.

45. Torii, T., Yoshimura, T., Narumi, M., Hitoshi, S., Takaki, Y., Tsuji, S., and Ikenaka, K. (2014). Determination of major sialylated N-glycans and identification of branched sialylated N-glycans that dynamically change their content during development in the mouse cerebral cortex. Glycoconj. J. *31*, 671–683. https://doi.org/10.1007/s10719-014-9566-2.

46. Govind, A.P., Jeyifous, O., Russell, T.A., Yi, Z., Weigel, A.V., Ramaprasad, A., Newell, L., Ramos, W., Valbuena, F.M., Casler, J.C., et al. (2021). Activity-dependent Golgi satellite formation in dendrites reshapes the neuronal surface glycoproteome. Elife *10*, e68910. https://doi.org/10.7554/eLife.68910.

47. Bonfanti, L. (2006). PSA-NCAM in mammalian structural plasticity and neurogenesis. Prog. Neurobiol. *80*, 129–164. https://doi.org/10.1016/j.pneurobio.2006.08.003.

48. Schindelin, J., Arganda-Carreras, I., Frise, E., Kaynig, V., Longair, M., Pietzsch, T., Preibisch, S., Rueden, C., Saalfeld, S., Schmid, B., et al. (2012). Fiji: an open-source platform for biological-image analysis. Nat. Methods *9*, 676–682. https://doi.org/10.1038/nmeth.2019.

49. Andres-Alonso, M., Ammar, M.R., Butnaru, I., Gomes, G.M., Acuña Sanhueza, G., Raman, R., Yuanxiang, P., Borgmeyer, M., Lopez-Rojas, J., Raza, S.A., et al. (2019). SIPA1L2 controls trafficking and local signaling of TrkB-containing amphisomes at presynaptic terminals. Nat. Commun. *10*, 5448. https://doi.org/10.1038/s41467-019-13224-z.

50. Haeussler, M., Schönig, K., Eckert, H., Eschstruth, A., Mianné, J., Renaud, J.B., Schneider-Maunoury, S., Shkumatava, A., Teboul, L., Kent, J., et al. (2016). Evaluation of off-target and on-target scoring algorithms and integration into the guide RNA selection tool CRISPOR. Genome Biol. *17*, 148. https://doi.org/10.1186/s13059-016-1012-2.

51. Borgmeyer, M., Coman, C., Has, C., Schött, H.F., Li, T., Westhoff, P., Cheung, Y.F.H., Hoffmann, N., Yuanxiang, P., Behnisch, T., et al. (2021). Multiomics of synaptic junctions reveals altered lipid metabolism and signaling following environmental enrichment. Cell Rep. *37*, 109797. https://doi.org/10.1016/j.celrep.2021.109797.

52. Slot, J.W., and Geuze, H.J. (2007). Cryosectioning and immunolabeling. Nat. Protoc. *2*, 2480–2491. https://doi.org/10.1038/nprot.2007.365.

53. Seidenbecher, C.I., Landwehr, M., Smalla, K.H., Kreutz, M., Dieterich, D.C., Zuschratter, W., Reissner, C., Hammarback, J.A., Böckers, T.M., Gundelfinger, E.D., and Kreutz, M.R. (2004). Caldendrin but not calmodulin binds to light chain 3 of MAP1A/B: an association with the microtubule cytoskeleton highlighting exclusive binding partners for neuronal Ca(2+)-sensor proteins. J. Mol. Biol. *336*, 957–970. https://doi.org/10.1016/j.jmb.2003.12.054.

54. Church, G.M., and Gilbert, W. (1985). The genomic sequencing technique. Prog. Clin. Biol. Res. *177*, 17–21.

55. Gubelmann, C., Gattiker, A., Massouras, A., Hens, K., David, F., Decouttere, F., Rougemont, J., and Deplancke, B. (2011). GETPrime: a gene- or transcript-specific primer database for quantitative real-time PCR. Database (Oxford) *2011*, bar040. https://doi.org/10.1093/database/bar040.

56. Schiff, M., Weinhold, B., Grothe, C., and Hildebrandt, H. (2009). NCAM and polysialyltransferase profiles match dopaminergic marker gene expression but polysialic acid is dispensable for development of the midbrain dopamine system. J. Neurochem. *110*, 1661–1673. https://doi.org/10.1111/j.1471-4159.2009.06267.x.

57. Pfaffl, M.W., Horgan, G.W., and Dempfle, L. (2002). Relative expression software tool (REST) for group-wise comparison and statistical analysis of relative expression results in real-time PCR. Nucleic Acids Res. *30*, e36. https://doi.org/10.1093/nar/30.9.e36.

58. Morellini, F., Lepsveridze, E., Kähler, B., Dityatev, A., and Schachner, M. (2007). Reduced reactivity to novelty, impaired social behavior, and enhanced basal synaptic excitatory activity in perforant path projections to the dentate gyrus in young adult mice deficient in the neural cell adhesion molecule CHL1. Mol. Cell. Neurosci. *34*, 121–136. https://doi.org/10.1016/j.mcn.2006.10.006.

59. Evers, M.R., Salmen, B., Bukalo, O., Rollenhagen, A., Bösl, M.R., Morellini, F., Bartsch, U., Dityatev, A., and Schachner, M. (2002). Impairment of L-type Ca2+ channel-dependent forms of hippocampal synaptic plasticity in mice deficient in the extracellular matrix glycoprotein tenascin-C. J. Neurosci. *22*, 7177–7194.

STAR★METHODS

KEY RESOURCES TABLE

REAGENT or RESOURCE	SOURCE	IDENTIFIER
Antibodies		
Rabbit anti-Clathrin Heavy Chain (P1663)	Cell Signaling	Cat#2410S; RRID: AB_2083156; ICC 1:300
Guinea pig anti-Shank3	Synaptic Systems	Cat#162304; RRID: AB_2619863; IHC 1:30; ICC 1:1000
Mouse anti-MAP2	Sigma	Cat#M4403; RRID: AB_477193 IHC 1:500
Guinea pig anti-MAP2	Synaptic Systems	Cat# 188004; RRID: AB_2138181 ICC 1:500
Guinea pig anti-Giantin	Synaptic Systems	Cat#263004; RRID: AB_2619983 ICC 1:500; IHC 1:300
Mouse anti-VPS35	Santacruz	Cat#sc-374372; RRID: AB_10988942 IHC 1:300
Rabbit anti-ERGIC53	Sigma	Cat#E−1031; RRID: AB_532237; IHC: 1:300
Mouse anti-GM130	Abcam	Cat#ab52649; RRID: AB_880266 ICC 1:1000; IHC 1:500
Rabbit anti-GFP	Abcam	Cat#ab6556; RRID: AB_305564 ICC 1:1000
Rabbit anti-RFP	Rockland	Cat#600-401-379; RRID:2209751 ICC 1:1000; IHC 1:500
Rabbit anti-M6PR	Abcam	Cat# ab124767 ICC 1:500
Rabbit anti-Syntaxin 6	Synaptic Systems	Cat#110 062; RRID: AB_887854 ICC 1:500
Mouse anti-Syntaxin 6	BD Biosciences	Cat#610635; RRID: AB_397965 ICC 1:500; IHC 1:500
Mouse anti-NCAM	Abcam	Cat#ab9018; RRID: AB_306945 IHC 1:500
Mouse anti-Polysialic Acid-NCAM (PSA-NCAM)	Millipore	Cat#MAB5324; RRID: AB_95211 IHC 1:500
Rat monoclonal anti-HA (3F10)	Fischer Scientific	Cat#50-100-3325; RRID: ICC:1:1000
Anti-mouse-AlexaFluor 405	ThermoFisher Scientific	Cat#A-31553; RRID: AB_221604; IF-1:300
Anti-rabbit Alexa Fluor 488	ThermoFisher Scientific	Cat#A-11001; RRID: AB_2534069 ICC 1:500
Anti-mouse-AlexaFluor 568	ThermoFisher Scientific	Cat#A-11004; RRID: AB_2534072 ICC- 1:500
Anti-guinea pig-AlexaFluor 647	ThermoFisher Scientific	Cat#A-21235; RRID: AB_2535804 IF- 1:500
Anti-rabbit-IgG-HRP	Dianova	Cat#111-035-114 1:20000
Anti-mouse-IgG-HRP	Dianova	Cat#115-035-146 1:20000
RFP-Booster Atto580	Nanotag	Cat#N0401-Ab580-L 1:250
Streptavidin conjugated with Alexa Fluor® 647	ThermoFisher Scientific	Cat#S21374 ICC: 1:1000
4′,6-diamidino-2-phenylindole (DAPI)	Biozol	Cat#BCL-BCFA-211; IHC:1:1000
Bacterial and virus strains		
pAAV9-Syn-pGolt-mCherry	This study	N/A
pAAV9-CaMKII-Cre	James M. Wilson (unpublished)	Addgene #105558

(*Continued on next page*)

Continued

REAGENT or RESOURCE	SOURCE	IDENTIFIER
pAAV9-Ef1α-loxP-EGFP-loxP	This study	N/A
Chemicals, Peptides, and Recombinant Proteins		
Tunycamicin	Tocris Bioscience	Cat#3516
Lipofectamin 2000	Invitrogen	Cat#11668027
ConA-biotin (Concanavalin A biotinylated, from *Canavalia ensiformis* (Jack bean)	Sigma-Aldrich	Cat#C2272 ICC: 0.33 μg/ml
WGA-biotin (Lectin from *Triticum vulgaris*)	Sigma-Aldrich	Cat#L5142 ICC: 0.40 μg/ml
HPL-biotin (Lectin from *Helix pomatia*)	Sigma-Aldrich	Cat#L6512 ICC: 0.35 μg/ml
Ac4GlcNAz	Jena Biosciences	Cat#CLK-1085
Ac4ManNAz	Jena Biosciences	Cat#CLK-1084
Ac4GalNAz	Jena Biosciences	Cat#CLK-1086
DBCO-AF488	Jena Biosciences	Cat#CLK-1278
Experimental Models: Cell Lines		
HEK293T	ATCC	CRL-3216
Experimental Models: Organisms/Strains		
Mouse: Caln-1$^{-/-}$	This paper	N/A
Mouse: mGolt	This paper	N/A
Winstar Rats	Janvier	RjHan:WI
Oligonucleotides		
Primer for cloning CDMPR_fow: AATAGAA TTCGCCACCATGAAGACGATC	This paper	N/A
Primer for cloning CDMPR/CIMPR_rev: TAGCGGCCGCTCCGGATCCGTTAATTAATTATCA	This paper	N/A
Primer for cloning CIMPR_fow: AATAGAATTCACCATGCTGGTGCAAGGCAG	This paper	N/A
Primer for cloning NCAM (The RUSH system) NCAM fwd ATGC TGC GAA CTA AGG ATC TC	This paper	N/A
Primer for cloning NCAM (The RUSH system) NCAM rev TGC TTT GCT CTC ATT CTC TTT C	This paper	N/A
Primer for cloning St8SiaII-GFP St8SiaII-fwd ATGCAGCTGCAGTTCC	This paper	N/A
Primer for cloning St8SiaII-GFP ST8SiaII-rev GGT ACC CTA TTT ATT ACA ACT	This paper	N/A
Primer for qPCR Caln1_81_for:CAACCG ATCTCTGTCTGCA	This paper	N/A
Primer for qPCR Caln1_81_rev: GCTTCT CGGATTTCATCCAG	This paper	N/A
Primer for qPCR Actin_for: CACTGTCGA GTCGCGTCC	This paper	N/A
Primer for qPCR Actin_rev: TCATCCATG GCGAACTGGTG	This paper	N/A
Primer for qPCR Caln2_86_rev: CTTCAT GGACAAGTGCTCG	This paper	N/A
Primer for qPCR Caln2_86_for:TCTGGAA GTGTGACATGCA	This paper	N/A
Primer for genotyping: Calneuron_fwd: CCCTAAAATCAATTAGG AGTTATTCAAGTGATGG	This paper	N/A
Primer for genotyping: Calneuron_rev: CACACCTAGTCCTAGCT AATCAACGCTC	This paper	N/A

(*Continued on next page*)

Continued

REAGENT or RESOURCE	SOURCE	IDENTIFIER
Primer for genotyping: mGolt_fwd: GGCGAG TTCATCTACAAGGTGAAGCTG	This paper	N/A
Primer for genotyping: mGolt_rev: GACACTG ATGATGAAGGCGATGGCGA	This paper	N/A
Sg-Caln1-Nterm-1: GAAATTAATACGACTCA CTATAGGGAGAGTACAACATGTATGCATGTGCGT TTTAGAGCTAGAAATAGCAAGTTAAAATAAGGC	This paper	N/A
Sg-Caln1-Nterm-2: GAAATTAATACGACTCACTATA GGGAGAGTTACCACCCTATGAATCCCAGTTTTA GAGCTAGAAATAGCAAGTTAAAATAAGGC	This paper	N/A
Sg-Caln1-Cterm-1: GAAATTAATACGACTCACTATA GGGAGAGTTGGCAGTTAGGGCTAAGTAGTTTTAG AGCTAGAAATAGCAAGTTAAAATAAGGC	This paper	N/A
Sg-Caln1-Cterm-2: GAAATTAATACGACTCACTATA GGGAGAGGTTGCCTTGGATACTGATTGTTTTAG AGCTAGAAATAGCAAGTTAAAATAAGGC	This paper	N/A
Recombinant DNA		
EGFP N1	Clontech	Cat#6085-1
PSI-HIV-H1 – panCalneuron KD and scrambled	[33]	N/A
pCMV-pGolt-mCherry	[13]	N/A
pSyn-pGolt-mCherry	[13]	N/A
pCMV-Str-KDEL(The RUSH System – Hook)	[22,31]	Addgene #65306
pCMV-NCAM180-GFP-RUSH	This study	N/A
pCMV-CDMPR-GFP	This study	N/A
pCMV-CIMPR-GFP	This study	N/A
pSyn-St8SiaII-GFP	This study	N/A
Software and algorithms		
Fiji	[48]	http://fiji.sc/; RRID: SCR_002285
GraphPad Prism v8	GraphPad	http://www.graphpad.com/scientific-software/prism/
Imaris 9.2	Bitplane	http://www.bitplane.com/imaris/imaris RRID: SCR_007370

RESOURCE AVAILABILITY

Lead contact

Further information and requests for resources and reagents should be directed to and will be fulfilled by the lead contact, Dr. Michael R. Kreutz (michael.kreutz@zmnh.uni-hamburg.de).

Materials availability

All constructs and material are available upon request to the lead contact.

Data and code availability

- All data reported in this paper is available upon request to the lead contact.
- This paper does not report original code.
- Any additional information required to reanalyze the data reported in this paper is available upon request to the lead contact.

EXPERIMENTAL MODEL AND STUDY PARTICIPANT DETAILS

Animals were maintained in the animal facility of the Leibniz Institute for Neurobiology, Magdeburg (Germany) or ZMNH, Hamburg (Germany) under controlled environmental conditions. All animal experimentation was performed in accordance with the ARRIVE guidelines for animal experimentation, EU regulations and approved by the local ethical committee. C57BL/6J mice were housed

in C1ZMNHC1 or in the animal facility of the Leibniz Institute for Neurobiology, Magdeburg (Germany). Wistar rats were housed in the FTH of the UKE. Animals were housed at 22°C on a 12 h light/12 h dark cycle with *ad libitum* access to food and water in the breeding barriers of the Forschungstierhaltung of the University Medical Center Hamburg-Eppendorf. All experiments were approved by the local authorities of the State of Hamburg (Org 886; Nr.125/17). C57BL6J/UKE mice were used for mating and backcrossing.

Rat primary hippocampal culture

Primary rat hippocampal cultures were prepared from Wistar rat embryos of both sexes (E18). The rats were decapitated and hippocampi dissected. After treatment with trypsin at 37°C for 15 min and subsequent mechanical dissociation, cells were plated on 18 mm glass coverslips coated with poly-D-lysine at a density of 20.000–60.000 cells per well in DMEM medium (Gibco) supplemented with 10% fetal bovine serum (FBS), 0.5 mM Glutamax (Gibco). After 1h media was exchanged to BrainPhysTM neuronal medium (Stemcell Technologies) supplemented with 1X SM1 (Stemcell Technologies), 0.5 mM glutamine (Gibco). Cells were kept at 37°C, 5% CO_2 and 95% humidity until use.

Mouse hippocampal primary cultures

Tissue and cell preparation were carried out under the license number Org886. Hippocampal mouse cultures were prepared from mice of both sexes at postnatal day 0 or 1 as previously described.[49] Briefly, mice were decapitated and dissected hippocampi were collected in 450 μL HBSS. 50 μL Trypsin (0.25%Trypsin-EDTA) was added and the solution was kept at 37°C for 15 min. After two washes with HBSS, hippocampi were mechanically triturated in DMEM containing 10% FBS and 0.5mM glutamine. Cells were plated onto 18 mm glass coverslips coated with poly-L-lysine at a density of 80000 cell per well in a 12-well plate and cells were left at 37°C 5%CO2. Medium was exchanged after 1h for Neurobasal A (ThermoFisher) supplemented with B27 (Gibco) and Glutamax (ThermoFisher). Cells were fed once a week by removing 100 μL of medium and adding 200 μL of freshly prepared supplemented Neurobasal A.

Cell lines

Human embryonic kidney 293T cells (HEK293T) were cultured in DMEM supplemented with 10% FCS and 1% ml PenStrep.

METHOD DETAILS

Generation of transgenic mice

The reporter line mGolt was generated via pronucleus injection and random integration of the pGolt probe under control of the Synapsin promoter into the genome. In brief, C57BxCBA (= F1) or B6, 3–4 weeks old were superovulated by hormone injection. Embryos were isolated from the ampulla of the oviduct in drops of KSOM/HEPES containing 0.3 mg/mL hyaluronidase and cumulus cells were removed. Injections were performed using 2 ng/μL of isolated fragment diluted in 10 mM Tris, pH 7.4, 0.1 mM EDTA with the help of a Femtojet and micromanipulators (Eppendorf) using DIC optics of an Olympus microscope. Modified embryos were implanted into pseudo-pregnant foster mothers. Animals were sedated with 4% isoflurane and kept at 2% isoflurane throughout the surgery. Analgesia was carried out with Burprenorphin (0.05 mg/kg BW) before, and with Carprofen (5 mg/kg BW) after surgery. The bursa was opened above the infundibulum. The embryos were injected into the infundibulum and the wound was closed.

The *caln1* knockout mouse line was generated using the CRISPR-Cas9 system delivered by single-cell embryo electroporation. Single guide RNAs (sgRNAs) were designed using the CRISPOR program,[50] to bind upstream and downstream of the second exon, resulting in a full KO. The zygotes with clearly visible pronuclei were selected and they were taken up in KSOM. The selected zygotes were washed in OptiMEM at 4°C. sgRNAs (600 ng/μL) and Cas9 protein (IDT) were diluted in OptiMEM. 5μL of the solution was pipetted in the electroporation chamber. The electroporation was carried out with an NEPA21-electroporator (Nepagene).

For the mGolt mouse line 4 founders were tested for sufficient expression of the probe and 1 founder was used for the establishment of the line. For the *caln1* KO line, founders were backcrossed to C57BL6/J/UKE to avoid mosaicism and offspring exhibiting the correct genotype were then used to establish the KO line. The mGolt and *caln1* KO line were crossbred to generate *caln1*-GS line.

Transfection

Transfection of primary neurons was carried out at DIV14-16 as described previously[49,51] using Lipofectamine 2000 (Invitrogen) following manufacturer instructions. Experiments were performed the day after transfection, typically after ~16h. For experiments using the panCalneuron KD, neurons were transfected at DIV3 for Sholl analysis, and at DIV9 experiments in which the Golgi morphology and the spine density were analyzed. In all cases, cells were fixed 4–5 days after transfection.

Transfection of HEK293T cells was performed with MaxPEI (25000, Polysciences) according to manufacturer's instructions at about 60% confluency.

NCAM release with the RUSH system

The ER-retention using selective hooks (RUSH) system was used to visualize NCAM trafficking following its exit from the ER.[22,31] An ER-hook (Addgene #65306) consisting of the coding region of Streptavidin fused to a signal sequence and to a KDEL motif was co-expressed together with an expression vector containing a streptavidin binding peptide (SBP; Addgene 65304) fused to the target protein

NCAM180 and to a GFP and an HA tag for detection (SBP-GFP-HA-NCAM). The interaction between streptavidin and the SBP was interrupted by addition of 40 μM Biotin to the culture medium at 37°C. To control for the surface expression of the protein after release, a surface staining using an antibody against the HA-tag (Roche 11867423001, 1:500) was performed in culture medium for 10 min at 37°C. Imaging of fixed neurons was performed on a Leica SP8 X microscope controlled by the Leica LAS X software and equipped with a WLL 470–670 laser. Stack images were acquired with an 80 × 80nm pixel size, a 512x512 resolution, and a Z-step of 0.30μm. The live-imaging experiment of NCAM release in HEK cells was performed in a VisiScope TIRF/FRAP imaging system from Visitron Systems based on Nikon Ti-E. The system is equipped with the Perfect Focus System (Nikon), Nikon CFI Apo TIRF 100X, 1.49NA oil objective, a back focal TIRF scanner for suppression of interference fringes (iLas2, Roper Scientific), and controlled with VisiView software (Visitron Systems). Laser lines of 488 and 561 nm were used and fluorescence was collected through ET 488/561 Laser Quad Band filters to a The ORCA-Flash 4.0 LT sCMOS camera. Time-lapse images were acquired with a frequency of an image every 2 min in neuronal conditioned media.

Live-labeling, immunostaining, and imaging

Antibodies

Information regarding the antibodies used in this study is available in the key resources table.

Immunocytochemistry

Following fixation with 4% paraformaldehyde (PFA) and 4% sucrose for 15 min, cells were washed thoroughly three times with PBS and permeabilized with 0.2% Triton X-100 in PBS for 10 min. Cells were then incubated with blocking buffer (2% Glycine, 2% BSA, 0.2% gelatine and 50 mM NH4Cl). An alternative blocking buffer (10% HS and 0.1% Triton in PBS) was used for immunostaining of Golgi. Incubation with primary antibodies diluted in the corresponding blocking buffer was done overnight at 4°C. After three washes with PBS, secondary antibodies were applied diluted in blocking buffer and incubated for 1h at room temperature. Following three washes with PBS, coverslips were mounted onto glass slides using Mowiol (Carl Roth). For surface labeling the cells were incubated with the primary antibody in culture medium at 37°C for 10 min before fixation in PFA.

Immunohistochemistry (IHC)

IHC was carried out as previously described.[51] In brief; mice were perfused with 4% PFA in PBS and brains were subsequently post-fixed for 12h in 4% PFA. Cryoprotection was carried out in 15% sucrose followed by 30% sucrose. Brains were flash-frozen in −50°C 2-Methylbutane for 30 s and stored at −80°C. Cryosections of 20–40 μm thickness were prepared in a cryostat (HYRAX C 60) with MX35Ultra microtome blades. They were incubated in solution containing primary antibody in blocking buffer (10% NGS, 0.3% TX-100 in PBS) for 48 h at 4°C. Sections were then washed in PBS for 1h and incubated with 0.2% BSA/PBS for 1h. Incubation with secondary antibodies was performed for 2h at RT in blocking buffer. Sections were then washed 3 times and mounted in glass slides using Mowiol (Carl Roth).

Nissl staining

Cryosections were acidified in 0.05 M sodium acetate buffer (pH 4,0–4,2; adjusted with acetic acid) and subsequently stained in Cresylviolet (0,5v/v%) for 5–10 min. Dehydration was achieved by incubating the cryosections first in a 0.05M sodium acetate buffer for 3 minutes, followed by subsequent incubations in 50% ethanol, 70% ethanol and 96% ethanol for 2 minutes each. To clear the sections, they were twice incubated with 2/3 ethanol and 1/3 isopropanol for 5 minutes before they were subjected to 3 washes of 5 min each in Xylol before being mounted in glass slides using Mowiol.

Lectin staining

Primary cultures were treated with 0.6 μl AraC at DIV 3 to reduce glia content and fixed in 4% PFA between DIV 9 and 16. Cells were permeabilized using 0.2% Triton X-100 for 10 min at room temperature and endogenous biotin was chelated by using the Endogenous Biotin-Blocking Kit (ThermoFisher Scientific, #E21390) following manufacturer's instructions. After that, cells were incubated in blocking buffer 1 and the lectin labelling was carried out in parallel with antibody staining.

Click chemistry for glycosylation

Primary neurons were transduced with an AAV-Syn-pGolt-mCherry virus at DIV8 to efficiently label GS and cells were kept in at 37°C 5% CO2 until the experiment was done. At DIV 14, azide-functionalized monosaccharides (Ac4ManNAz, Ac4GlcNAz and Ac4GalNAz, Jena Biosciences) were added to the growing cells at a concentration of 1μM and neurons were returned to the incubator. Cells treated with DMSO were used as a negative control. After 24h, cells were incubated with 1μM DBCO-AF488 (Jena Biosciences) in growing medium for 40 min at 37°C. Cells were washed three times with pre-warmed PBS before fixation with 4% PFA. Images were acquired in a Leica TCS SP5 scanning microscope controlled by Leica LAS AF software using HCX PL APO63x1.40. Stack images of secondary dendrites were acquired using the 488, 568 and 635 nm laser lines (12-bits, 80 × 80nm pixel size, 1000 Hz, Z-step 0.29 μm). Fluorescence was collected using three HyD detectors.

Image acquisition

Unless otherwise indicated, imaging of cryosections was performed with an Olympus Fluoview FV1000 microscope using an oil immersion objective (60×/1.40). Stack of images were acquired at 640x640 resolution, at a zoom 4, 80 × 80 nm pixel size and a Z-step of 0.30μm. Images were acquired using the 405, 488 and 568 nm laser lines.

Regions of interest were acquired in the central region of the CA1 and CA1 strata were categorized as following: SRP was defined as the area directly adjacent to the visible somas of the stratum pyramidale; SRD was defined as the area below the SLM characterized by morphologically straight dendrites running in parallel; the SLM was defined as the more distal part of the pyramidal neurons in which dendrites branch to run typically perpendicular to the main apical dendrites.

Unless otherwise indicated, imaging of fixed primary neurons was performed on a Leica SP8 X microscope controlled by the Leica LAS X software and equipped with a WLL 470-670 laser. Stack images were acquired with an 80x80nm pixel size, a 512x512 resolution, and a Z-step of 0.30μm.

In all experiments, image acquisition settings were optimized and kept constant for all images and experimental groups within each data set. Raw images were used for quantification. Representative images displayed in figures were treated with a Gaussian blur with a sigma radius of 0.6, cropped, and each color channel was adjusted linearly in Fiji.[48]

Image analysis

Unless otherwise stated, images were analyzed as following. First, image background was removed from raw images using the Subtract function of the Fiji software.[48] For colocalization analysis, images were binarized and masks of labeled structures were obtained from each fluorescent channel using Fiji.[48] The masks were then compared and those structures whose masks were overlapping by at least one pixel were considered. For quantification of GS along dendrites, the MAP2 fluorescence signal was masked to indicate dendritic localization.

For assessing the colocalization between the lectin labeling and pGolt-mCherry (Figures 2A and 2B), raw images were analyzed using the built-in spot detection algorithm available in Imaris 9.2. (RRID: SCR_007330). Spots were generated independently in each channel and they were subsequently overlaid. Spots generated in the GS that were at least partially colocalizing with spots generated in the lectin channel were considered as positive for the second marker.

Electron microscopy

Postembedding CLEM labeling

Mice were deeply anesthetized and transcardially perfused with a mixture of 4% PFA and 0.1% glutaraldehyde (GA) in 0.1 M phosphate buffer (PB) at pH 7.4. 100 μm thick sagittal vibratome sections of the brains were cut with a Vibratome VT 1000S (Leica Biosystems Nussloch, Germany). For postembedding CLEM labeling, small pieces of cryoprotected (2.3 M sucrose) hippocampal CA1 regions were mounted on specimen holders and immersed in liquid nitrogen. Ultrathin sections (60 nm) were cut and labeled according to.[52] Briefly, sections were collected on Carbon-Formvar-coated nickel grids (Science Services GmbH, Germany). Antibodies, rabbit anti-RFP (1:100) and mouse anti MAP2 (1:500), were first recognized with Alexa 488 and Alexa 546 respectively and RFP was further detected with Protein A coupled to 10- or 15 nm large colloidal gold particles (purchased from G. Posthuma, University Medical Center Utrecht). Grids were embedded in 50% glycerol on an object slide with sections facing up and covered carefully with a coverslip. Images of labeled dendrites and RFP-positive spots were taken at an Olympus Fluoview 1000 confocal microscope. Altogether >3 independent experiments with 2 EM Grids each were performed. Section overviews of the CA1 region were taken and parts of distal dendrites ranging from 10 to 15 μm length were imaged with a 5 time Zoom and 60x oil immersion objective. Thereafter the grids were unmounted with distilled water stained with Uranylacetate for 5 minutes and dried by the looping out method. Ultrathin sections (60 nm) were examined in a TEM 2100Plus (Jeol, Japan). Images were acquired with the XAROSA CMOS camera (Emsis, Germany).

Biochemistry

Protein measurement

Protein concentrations were measured using amido black. A standard curve was established using defined concentrations of bovine serum albumin (BSA). Amido black was added to the protein samples and the controls and incubated for 20 min at RT in a 96-well plate. The wells were washed 3x in methanol-acetic acid solution. The wells were air dried and dissolved in 300 μl of methanol-acetic acid solution by shaking for 30 min. The optic density was measured at 620 nm with Fluoro Star Optima Flurimeter (BMG Labtechnologies, Offenburg, Germany). The protein concentrations were calculated based on the BSA standard curve.

SDS-PAGE

SDS-PAGE and western blot were conducted according to.[53] SDS-PAGE was performed on 5% to 20% gradient gels. The probes were dissolved in SDS sample buffer. The gel run was run at 12 mA per gel at 4°C.

Immunoblotting

Immunoblotting was at 200 mA for 2 h (minimum of 60 V), on nitrocellulose or PVDF membranes. The efficiency of the transfer was controlled by staining the membrane with Ponceau solution for 5 min. The membranes were blocked with 5% (m/v) milk powder or BSA in TBS-T. The blocking buffer was adjusted to each individual primary antibody for minimal unspecific binding. The membranes were incubated with the primary antibody in TBS-A overnight at 4°C under light shaking. They were washed 10 min in TBS, 10 min in TBS-T, 5 min TBS-T and 5 min TBS followed by incubation with the HRP-coupled secondary antibody in the blocking buffer. Washes were performed for 10 min in TBS and in TBS-T, and for 5 min TBS-T and 5 min TBS. To develop the signal, ECL solution (Pierce, Rockford, USA) was used and the image was acquired with Intas ECL chemocam imager (Licor, Cambridge, UK).

Southern blot

Southern blotting was performed with the alkaline methods published in,[54] using Hybond-N membranes. The membrane was exposed on a phospho imager plate overnight which was scanned in the BAS-reader using the TINA0209 program.

qPCR

RNA extraction was performed using a GenUP Total RNA kit from a half hippocampus (left) of 5 12-weeks old KO mice and their corresponding WT littermate controls. The samples were homogenized by vigorous shearing of the tissue in 700 μl lysis buffer with 10 strokes of a 1ml syringe equipped with a 20 and 23 gauche canula. Column- based purification was performed according to the instructions given for the kit. Total RNA was eluted in nuclease-free buffer and photometrically quantified using a NanoDrop 2000 (Thermo Fisher Scientific). RNA integrity was assessed by inspection of 18S and 28S ribosomal RNA bands using agarose gel-electrophoresis. For expression analysis residual genomic DNA was removed using ezDNase (VILO Mastermix with ezDNase kit, Invitrogen, Thermo Fisher Scientific). The same kit was used for reverse transcription using oligo dT primers as well as hexamer primers with 500 ng total RNA for each reaction, respectively, and according to the manufacturer's instructions.

RT-PCR reactions were performed with the PowerUp SYBR Green Mastermix (Life Technologies) according to the manufacturer's instructions using the following primers derived from GETPrime Database (GETPrime: 2439323; and GETPrime: 2495140)[55]: Caln1_81_for: CAACCGATCTCTGTCTGCA; Caln1_81_rev: GCTTCTCGGATTTCATCCAG; Caln2_86_for: TCTGGAAGTGT GACATGCA; Caln2_86_rev: CTTCATGGACAAGTGCTCG. Primer sequences for NCAM, St8SiaII and St8siaIV were the same as in.[56]

Normalization of qPCR-based mRNA expression analyses was performed by using Actin (GenBank: NM_007393.5, base 29 to base 117) using the following validated primers: Actin_for: CACTGTCGAGTCGCGTCC; Actin_rev: TCATCCATGGCGAACTGGTG. Differential gene expression was calculated with the Relative Quantification app (Relative Quantification, version 3.8, Thermo Fisher), using the individually determined efficiencies of the respective targets for the ΔΔ-Ct determinations and the REST software was used for the evaluation of the significance of the difference.[57]

Electrophysiology

Preparation of hippocampal slices

Hippocampal slices were prepared from 5- to 6-month-old *Caln-1* ko and age-matched wt male mice as previously described.[58] Briefly, animals were deeply anesthetized with isoflurane and then immediately decapitated. The brain was removed and cut in two hemispheres. 350 μm-thick slices weroe cut horizontally by a Vibroslicer (Leica, Nussloch, Germany) in ice-cold sucrose-based solution containing (in mM): 250 sucrose, 25 NaHCO3, 25 glucose, 2.5 KCl, 1.25 NaH2PO4, 2 CaCl2, 1 MgCl2 (pH 7.3, adjusted with NaOH). Slices were transferred and kept at room temperature in a large chamber (500 ml) filled with carbogen-bubbled artificial cerebrospinal fluid (ACSF) containing (in mM): 125 NaCl, 25 NaHCO3, 25 glucose, 2.5 KCl, 1.25 NaH2PO4, 2 CaCl2, 1 MgCl2 (pH 7.3, adjusted with NaOH) for at least two hours before recording. Slices were transferred into a submerged-type recording chamber for recordings of field excitatory post-synaptic potentials (fEPSPs) in ACSF.

Analysis of basal transmission and plasticity

Glass electrodes filled with ACSF were used for stimulation and recording of fEPSPs. Stimulation current pulses of 0.2 ms were applied via monopolar stimulating glass electrodes with a broken tip and resistance of < 1 MΩ.

Stimulus–response curve has been obtained by applying current pulses of increasing amplitude and measuring the amplitude of evoked responses. The stimulation intensity was determined based on the stimulus-response curve to elicit fEPSPs with an amplitude of ∼30 % and ∼50 % of the supramaximal fEPSP for recordings of the paired-pulse facilitation (PPF) and long-term potentiation (LTP), respectively.

PPF was induced by paired-pulse stimulation and defined as the ratio between the amplitudes of the fEPSPs evoked by the second and first pulses delivered with 10, 20, 50, 100 and 200 ms intervals. LTP was induced by two trains of high-frequency stimulation (HFS). Each train included 100 pulses delivered at 100 Hz. Inter-train interval was 20 s and duration of pulses was 0.2 ms.[59] The LTP value was calculated as the mean amplitude of fEPSPs recorded 50-60 min after HFS relative to the mean amplitude of fEPSPs recorded during 10 min preceding HFS.

For analysis of synaptic transmission and plasticity at CA3-CA1 synapses, the stimulating and recording electrodes were placed in the stratum radiatum of the CA1 region (Figures 4G–4I, S4D, and S4E).

For recording of fEPSP elicited by stimulation of temporoammonic (TA) projections from the entorhinal cortex in the CA1, stimulating and recording electrodes were placed in the stratum lacunosum–moleculare of the CA1 (Figures 4G, 4J, 4K, S4F, and S4G). LTP was induced with the stimulus intensities eliciting fEPSPs with the amplitudes of 50% and 100% of the supramaximal fEPSP in CA3-CA1 and TA-CA1 connections, respectively. In the latter case, 100 μM picrotoxin was applied to the slices 10 min before and during HFS to disinhibit slices and facilitate induction of this form of LTPs as previously described.[58] To avoid the effects of polysynaptic activation, the CA3 region was cut off.[40]

To measure the magnitudes of fast AMPAR- and slow NMDAR-mediated components in the composite fEPSPs at the TA-CA1 synapses, first, the composite fEPSPs were recorded for 10 min every 20 s in the ACSF containing 0.5 mM Mg^{2+} and in the presence of antagonists for GABAA (picrotoxin, 100 μM) and $GABA_B$ (CGP55845, 2 μM). The stimulation intensity was adjusted to elicit fEPSPs with an amplitude of 50% of the supramaximal fEPSPs. Thereafter, slices were incubated with NMDAR blockerAPV (50 μM) to assess the contribution of AMPARs. The mean NMDAR-mediated fEPSP was then obtained by subtraction of mean AMPAR-mediated fEPSP from the mean composite fEPSP. The areas of fEPSPs corresponding to fixed 5 ms and 10 ms time-windows around peaks of NMDAR and AMPAR components were used to calculate the ratio between components.

All recordings were obtained at room temperature using an EPC-10 amplifier (HEKA Elektronik, Germany). The recordings were filtered at 1 kHz and digitized at 10–20 kHz.

Spine count in CA1 pyramidal neurons

The following virus were produced in the UKE Vector Facility: AAV9-Ef1α-loxP-EGFP-loxP and AAV9-CaMKII-Cre, which was a gift from James M. Wilson (Addgene plasmid #105558, http://n2t.net/addgene:105558; RRID:Addgene_105558). For injection, a virus-containing solution was prepared using a 1:1 ratio of the AAV9-Ef1α-loxP-EGFP-loxP and AAV9-CaMKII-Cre, the latter being diluted 1:50.0000 in PBS. 12-14 week-old animals were anesthetized with 2.2–2.5% isoflurane and transferred to a stereotaxic apparatus (Stoelting), where they were maintained under isoflurane anesthesia (1–2%) with a single injection of Meloxicam (2mg/kg bw, s.c) for analgesia. After hair removal and disinfection of the scalp with ethanol, a midline incision was made into the skin. Bregma and Lambda coordinates were determined, and adjustments in head position were made to match the DV coordinates. Virus was injected into the dorsal hippocampal CA1 at AP −2.7, ML −2.75 or +2.75, and DV −1.25. A small burr hole was drilled into the skull (HM1 009, Meisinger) and 1 μl of virus-containing solution was injected into each hemisphere using the blunt needle of a Nanofil syringe and the UMP3T-2 (WPI) injection system with an injection rate of 75 nl/minute. Afterwards, the skin was sutured and the mouse was put under a heat lamp to allow for undisturbed recovery, before being returned to its home cage. Post-surgical analgesia was insured for three days with Meloxicam (2mg/kg bw; s.c.; 12h post surgery) and Carprofen (5mg/kg bw; p.o.; b.i.d.), respectively. Animals were group housed for 2 weeks after surgery to allow for viral-mediated gene expression. Afterwards, mice were transcardially perfused with 0.9% sodium cloride followed by 4% PFA, brains were extracted and fixed overnight in 4% PFA, before being transferred to 1% PFA for storage on the next day. Coronal sections of 300 μm were cut in a vibrotome and they were mounted onto glass coverslips using Mowiol. Stack images were acquired in a Leica TCS SP5 scanning microscope controlled by Leica LAS AF software using HCX PL APO63x1.40 using the 488 nm laser line (1024x1024 resolution, zoom 6, 40 x 40 nm pixel size, 1400 Hz, Z-step 0.29 μm). Fluorescence was collected using a HyD detector. CA1 strata were identified as explained above. Image analysis was performed using the IMARIS software.

QUANTIFICATION AND STATISTICAL ANALYSIS

Graphs and statistical analysis were made using the GraphPad Prism (GraphPad Software). Statistical tests used for each experiment are described within figure legends. The number of subjects considered for statistical comparison is described in graphs and/or figure legends associated with each experiment. P values >0.05 were considered as non-significant; p values <0.05 were considered significant (*); p<0.01 (**); p< 0.001 (***).